SPATIAL DECONFOUNDER: INTERFERENCE-AWARE DECONFOUNDING FOR SPATIAL CAUSAL INFERENCE

Ayush Khot[*]
Department of Computer Science
University of Illinois at Urbana-Champaign
akhot2@illinois.edu

Miruna Oprescu[*]
Department of Computer Science
Cornell University, Cornell Tech
amo78@cornell.edu

Maresa Schröder
LMU Munich
Munich Center for Machine Learning (MCML)
maresa.schroeder@lmu.de

Ai Kagawa & Xihaier Luo
Computing and Data Sciences
Brookhaven National Laboratory
{aik, xluo}@bnl.gov

ABSTRACT

Causal inference in spatial domains faces two intertwined challenges: (1) unmeasured spatial factors, such as weather, air pollution, or mobility, that confound treatment and outcome, and (2) interference from nearby treatments that violate standard no-interference assumptions. While existing methods typically address one by assuming away the other, we show they are deeply connected: *interference reveals structure* in the latent confounder. Leveraging this insight, we propose the **Spatial Deconfounder**, a two-stage method that reconstructs a substitute confounder from local treatment vectors using a conditional variational autoencoder (CVAE) with a spatial prior, then estimates causal effects via a flexible outcome model. We show that this approach enables nonparametric identification of both direct and spillover effects under weak assumptions—without requiring multiple treatment types or a known model of the latent field. Empirically, we extend `SpaCE`, a benchmark suite for spatial confounding, to include treatment interference, and show that the Spatial Deconfounder consistently improves effect estimation across real-world datasets in environmental health and social science. By turning interference into a multi-cause signal, our framework bridges spatial and deconfounding literatures to advance robust causal inference in structured data.

1 INTRODUCTION

Causal inference in spatial settings is critical for science and policy, from estimating the health effects of pollution to evaluating land use, climate interventions, and the spread of infectious disease. Most data in these domains are observational, since large-scale interventions are typically infeasible or unethical, so robust methodology is needed to draw valid conclusions. Yet observational studies in these settings face two fundamental challenges that standard methods rarely address together: (1) *spillover (interference)*, where the treatment at one site affects outcomes at nearby sites, violating the Stable Unit Treatment Value Assumption (SUTVA), and (2) *spatially structured unobserved confounding*, where latent fields such as weather or socioeconomic context jointly drive exposures and outcomes. Both are pervasive, and ignoring either leads to biased conclusions.

Consider air quality and health: respiratory mortality rates depend on local pollution and on neighboring regions' pollution due to transport and mobility, while latent meteorological factors such as temperature and humidity confound both. Any method that neglects interference or hidden confounders risks misleading the decisions policy-makers rely on for regulation and public health.

Existing approaches fall into two camps. Spatial causal methods model spillovers using exposure mappings or autoregressive dependencies but assume all relevant confounders are observed (Hudgens and Halloran, 2008; Forastiere et al., 2021). Confounding-adjustment methods

---

[*]Equal contribution. Correspondence to: amo78@cornell.edu.

—splines, matching, instrumental variables (IVs) (Dupont et al., 2022; Papadogeorgou et al., 2019; Papadogeorgou and Samanta, 2023)—address hidden bias by assuming explicit smooth field priors or exclusion restrictions, but treat interference as a nuisance. Separately, the *deconfounder* framework (Wang and Blei, 2019) shows that when each unit receives multiple causes, their joint distribution can reveal latent confounders. However, these methods are designed for i.i.d. data with simultaneous treatments—not spatial domains with localized interactions.
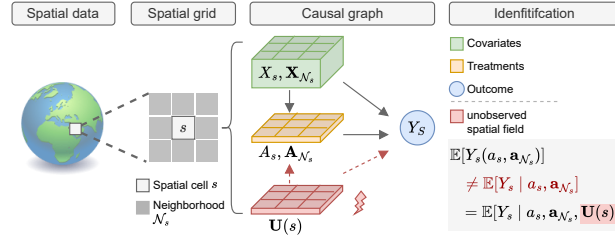

Figure 1: **Schematic of spatial interference/confounding**. Spatial data is represented in geographical cells indexed by site s with neighborhood $\mathcal{N}_s$. The outcome at s (e.g., mortality rate) is affected by the treatments (e.g., air quality) and observed confounders (e.g., demographic informataion) at both s and $\mathcal{N}_s$. However, unobserved latent factors (e.g., humidity) can confound the relationship, rendering causal effects unidentifiable.

We close this gap with the **Spatial Deconfounder**. Our key insight is that interference *creates* the very multi-cause structure that deconfounders require: each unit receives its own treatment together with those of its neighbors, all shaped by the same latent spatial field. Rather than a nuisance, interference becomes a source of signal for recovering hidden confounders. Building on this, we develop a two-stage framework that first reconstructs a smooth substitute confounder using a conditional variational autoencoder (CVAE) with a spatial prior, then estimates direct and spillover effects via any flexible outcome model (e.g., U-Net, GNN). This enables causal identification without requiring multiple treatment types or explicit latent-field models. Our **contributions** are as follows:

1. We introduce the **Spatial Deconfounder**, the first framework to *jointly* address spatial interference and unmeasured confounding by treating neighborhood exposures as multi-cause signals.

2. We prove *identification* of direct and spillover effects under localized interference and a weak latent-field sufficiency assumption, without requiring a parametric model for the hidden process.

3. We extend the `SpaCE` benchmark to include structured interference and show, across climate-, health-, and social-science datasets, that our method consistently reduces bias relative to spatial autoregressive, matching, and spline-based baselines.

By leveraging interference as a lens into hidden structure, the Spatial Deconfounder bridges spatial causal inference and multi-cause deconfounding, opening a path to robust causal estimation in complex geographic systems.

2 RELATED WORK

We give a brief overview of the related literature here; see Section A for a comprehensive survey with an expanded discussion. Our Spatial Deconfounder sits at the intersection of three main literatures: (i) spatial causal inference under interference and spatially structured confounding, (ii) methods for deconfounding in general average treatment effect (ATE) estimation, and (iii) deep learning for spatial and latent structure modeling.

Classical spatial causal inference. Design- and model-based approaches assume exchangeability after conditioning on *observed* covariates (given an exposure mapping) (e.g., Hudgens and Halloran, 2008; Anselin, 1988; Hanks et al., 2015; Forastiere et al., 2021; Tchetgen Tchetgen et al., 2021). They capture spatial dependence (splines/RSR, SAR, GNNs; simulators for domain physics) but do not address *unobserved* spatial confounding.

Spatial confounding and bias-adjustment methods. Bias from *unmeasured* spatial structure is mitigated via latent spatial effects, orthogonalization (S2SLS/SPATIAL+), proximity-based matching, IVs, or Bayesian priors (e.g., Hodges and Reich, 2010; Dupont et al., 2022; Papadogeorgou et al., 2019; Angrist et al., 1996). These methods rely on explicit smooth-field models or IV assumptions (or strong priors); none are able to nonparametrically reconstruct the hidden confounder — a gap our Spatial Deconfounder fills.

ATE estimation under unobserved confounding. With unmeasured confounding, point identification typically fails. Sensitivity analyses yield assumption-indexed bounds, trading point identification for robustness (e.g., VanderWeele et al., 2015; Frauen et al., 2023). Another approach is to reconstruct the unobserved confounder via the *deconfounder* framework, which fits a factor model to multiple causes in order to infer a substitute for the latent confounder, thereby restoring point identification (Wang and Blei, 2019; Bica et al., 2020). However, existing deconfounders require many simultaneous causes and assume no interference. We invert this: interference itself yields multi-cause treatment vectors, enabling latent-field recovery even with a single treatment type.

Deep learning for spatial modeling. U-Nets, GNNs, and patch-wise transformers capture multi-scale and long-range spatial structure (e.g., Ronneberger et al., 2015; Kipf, 2016; Liu et al., 2021), yet remain predictive rather than identifying causal effects without added causal structure.

Deep latent-variable models. CVAEs and related deep generative models can recover latent factors from data (Kingma and Welling, 2013; Sohn et al., 2015). We adapt this idea to spatial interference: interference supplies a multi-cause signal to nonparametrically reconstruct a smooth latent confounder, enabling identification of direct and spillover effects without a specified latent field.

Positioning of our work. Most spatial–interference methods ignore unmeasured confounders or rely on strong priors, while "deconfounder" methods are not adapted to spatial settings. We close this gap by using interference as a multi-cause signal to nonparametrically reconstruct latent confounders, identifying direct and spillover effects without specifying a latent-field model.

3 BACKGROUND AND SETUP

Notation. We use uppercase letters (e.g., X) for random variables and lowercase letters (e.g., x) for their realizations. Bold symbols denote vectors. The distribution of X is written P_X, with subscripts omitted when clear from context.

Data structure: lattice, neighborhoods, and observed variables. We consider a rectangular lattice $\mathcal{S} = \{(i,j) \mid i \in [N_x], \, j \in [N_y]\}$, where each site $s = (i,j)$ indexes a geographic cell. For a fixed radius $r > 0$, we define the neighborhood of s using the ℓ_∞ metric,

$$\mathcal{N}_s = \{s' \in \mathcal{S} : \|s' - s\|_\infty \leq r, \, s' \neq s\}, \quad \text{where } \|s' - s\|_\infty = \max\{|i' - i|, |j' - j|\}. \tag{1}$$

Thus $\mathcal{N}_s$ is the $(2r+1) \times (2r+1)$ square centered at s, excluding s itself. We take r to be in *pixels* (multiples of the cell size), though it may also be specified as a physical distance and mapped to the grid resolution. Other shapes (e.g., ℓ_2 balls) are possible, but we use the square ℓ_∞ ball by default for computational convenience.

At each site s we observe covariates $\mathbf{X}_s \in \mathbb{R}^{d_x}$, a binary treatment $A_s \in \{0,1\}$, and an outcome $Y_s \in \mathbb{R}$. For a neighborhood $\mathcal{N}_s$, we write $\mathbf{X}_{\mathcal{N}_s} = \{\mathbf{X}_{s'} : s' \in \mathcal{N}_s\}$, and analogously $A_{\mathcal{N}_s}$ and $Y_{\mathcal{N}_s}$. Realizations are denoted in lowercase, e.g., $\boldsymbol{x}_s, a_s, y_s$, and $\boldsymbol{x}_{\mathcal{N}_s} = \{\boldsymbol{x}_{s'} : s' \in \mathcal{N}_s\}$. For clarity, we focus on binary treatments, but the framework extends to continuous or multi-valued treatments through standard generalizations of the potential outcomes framework.

Potential outcomes and interference. We adopt Rubin's potential outcomes framework (Rubin, 2005). Standard causal inference relies on SUTVA, which rules out interference, i.e., one unit's outcome cannot depend on others' treatments. In spatial settings, this assumption is often violated, since exposures spill over. We assume *localized interference*: the potential outcome at site s depends only on its own treatment and those of its neighbors,

$$Y_s(\mathbf{a}) = Y_s(a_s, \mathbf{a}_{\mathcal{N}_s}), \tag{2}$$

where $\mathbf{a}$ is the full treatment vector, a_s the treatment at s, and $\mathbf{a}_{\mathcal{N}_s} = \{a_{s'} : s' \in \mathcal{N}_s\}$. The observed data contain only the realized outcome $Y_s = Y_s(A_s, \mathbf{A}_{\mathcal{N}_s})$ under the assigned intervention.

Causal estimands. Let $\mathbf{a}_{\mathcal{N}_s}^{(1)}$ and $\mathbf{a}_{\mathcal{N}_s}^{(0)}$ be two realizations of the neighbor treatments. Our targets are (i) the *average direct effect*, which varies the unit's own treatment while holding neighbors fixed,

$$\tau_{\mathrm{dir}} = \mathbb{E}\big[Y_s(1, \mathbf{a}_{\mathcal{N}_s}) - Y_s(0, \mathbf{a}_{\mathcal{N}_s})\big], \tag{3}$$

and (ii) the *average spillover effect*, which varies neighbors' treatments while holding the unit fixed,

$$\tau_{\mathrm{spill}} = \mathbb{E}\big[Y_s(a, \mathbf{a}_{\mathcal{N}_s}^{(1)}) - Y_s(a, \mathbf{a}_{\mathcal{N}_s}^{(0)})\big], \qquad a \in \{0,1\}, \tag{4}$$

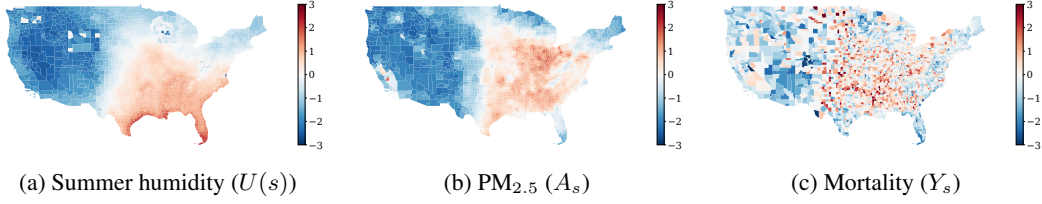| (a) Summer humidity ($U(s)$) | (b) PM$_{2.5}$ (A_s) | (c) Mortality (Y_s) |

Figure 2: Example spatial distribution of (normalized) confounder, treatment, and outcome in real-world dataset. The confounder $U(s)$ (summer humidity) varies smoothly across space, while the treatment A_s (PM$_{2.5}$) shows more local heterogeneity. The outcome Y_s (respiratory and cardiovascular mortality) reflects broader spatial health patterns.

with expectations taken over the observed joint distribution of $(\mathbf{X}_s, A_{\mathcal{N}_s})$.

Unobserved spatial confounding. To identify the treatment effects in Equations (3) and (4), one typically assumes *ignorability*: potential outcomes $Y_s(a_s, \mathbf{a}_{\mathcal{N}_s})$ are independent of treatment assignment given observed covariates $(\mathbf{X}_s, \mathbf{X}_{\mathcal{N}_s})$. This assumption cannot be tested from the data, and violations lead to biased causal estimates. In practice, many relevant drivers of exposure and outcome remain unobserved. We posit an unobserved spatial field $U : \mathcal{S} \to \mathbb{R}^{d_U}$ that captures latent influences such as topography, wind patterns, or socioeconomic context. Because $U(s)$ may affect both treatment and outcomes, we generally have

$$\text{Cov}(A_s, U(s)) \neq 0 \quad \text{and} \quad \text{Cov}(Y_s(a, \mathbf{a}_{\mathcal{N}_s}), U(s)) \neq 0, \tag{5}$$

where the covariances are understood component-wise when $U(s)$ is vector-valued. Thus, ignorability fails when conditioning only on $\mathbf{X}_s$ and $\mathbf{X}_{\mathcal{N}_s}$. In Section 5, we show that identification can nevertheless be recovered by leveraging mild smoothness assumptions on U together with our deconfounding procedure, which reconstructs a substitute for the latent field from observed treatment patterns.

Motivating example. Consider real environmental health data on a $0.25° \times 0.25°$ grid covering the continental United States. At each grid cell s, the treatment A_s indicates whether fine particulate matter (PM$_{2.5}$) exceeds the WHO guideline of 10 μg/m^3. Neighbor assignments are defined by a radius of one to two grid cells (roughly 25–50 km). The outcome Y_s is the rate of respiratory and cardiovascular mortality aggregated from hospital records. Latent factors can confound this relationship; for example, a meteorological driver such as humidity varies smoothly across space and may jointly influence both pollution exposures and health outcomes. Figure 2 illustrates treatment, outcome, and such a confounder for this dataset.

The remainder of the paper shows how the joint vector $(A_s, \mathbf{A}_{\mathcal{N}_s})$—a "multiple-cause" analogue supplied for free by interference—can be harnessed to reconstruct $U(s)$ and obtain unbiased estimates of Equations (3) and (4).
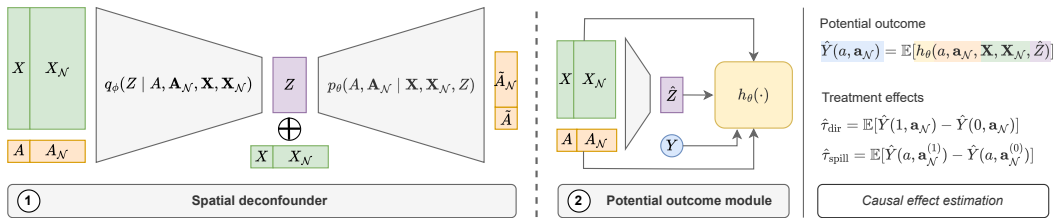
4 METHODOLOGY

Figure 3: **Architecture of the spatial deconfounder & estimation framework.** Stage ①: The CVAE takes treatments and observed confounders as input to learn the latent substitute confounder. Stage ②: We employ the reconstructed confounder together with the observed variables (now including the outcome) to train the potential outcome estimation module.

Algorithm 1 Spatial Deconfounder

Input: Spatial covariates $\{\mathbf{X}_s\}_{s \in \mathcal{S}}$, treatments $\{A_s\}_{s \in \mathcal{S}}$, outcomes $\{Y_s\}_{s \in \mathcal{S}}$, neighborhood radius r, grid Laplacian L
  1: **Stage ①: Confounder reconstruction (CVAE)**
  2: Define encoder $q_\phi(Z_s \,|\, A_s, A_{\mathcal{N}_s}, \mathbf{X}_s, \mathbf{X}_{\mathcal{N}_s}) = \mathcal{N}(\mu_\phi, \operatorname{diag} \sigma_\phi^2)$, decoder $p_\psi(A_s \,|\, \mathbf{X}_s, \mathbf{X}_{\mathcal{N}_s}, Z_s)$, and prior $p_\theta(Z) = \mathcal{N}(\mathbf{0}, \tau^{-1}(L + \epsilon I)^{-1})$.
  3: Minimize
  $$\mathcal{L}_A = \sum_s \mathbb{E}_{q_\phi}\big[-\log p_\psi(A_s \mid \mathbf{X}_s, \mathbf{X}_{\mathcal{N}_s}, Z_s)\big] \;+\; \sum_s D_{\mathrm{KL}}\big(q_\phi \,\|\, p_\psi\big),$$
  4: Set substitute confounder $\hat{Z}_s \leftarrow \mathbb{E}_{q_\phi}[Z_s]$ for all s.
  5: **Stage ②: Potential outcome module**
  6: Choose a spatial model h (e.g., U-Net) and fit by minimizing
  $$\mathcal{L}_Y = \sum_s \Big(Y_s - h(A_s, A_{\mathcal{N}_s}, \mathbf{X}_s, \mathbf{X}_{\mathcal{N}_s}, \hat{Z}_s)\Big)^2.$$
  7: Estimate effects by plug-in contrasts (Eq. 10).

As illustrated in Algorithm 1, our approach proceeds in two stages. First, we reconstruct a smooth substitute confounder from the joint distribution of local and neighbor treatments, using a conditional variational autoencoder (CVAE) that leverages interference as a multi-cause signal. Second, we feed the reconstructed confounder into a flexible potential outcome module for outcome modeling and effect estimation. This separation follows standard practice in deconfounding to prevent mediators from being inadvertently learned into the substitute confounder.

Stage ①: Confounder reconstruction. We model the assignment of treatments $\{A_s\}_{s \in \mathcal{S}}$ using an interference-aware CVAE. The encoder

$$q_\phi(Z_s \mid A_s, A_{\mathcal{N}_s}, \mathbf{X}_s, \mathbf{X}_{\mathcal{N}_s}) = \mathcal{N}\big(\mu_\phi(\cdot), \operatorname{diag} \sigma_\phi^2(\cdot)\big) \tag{6}$$

maps the local treatment and neighborhood treatments, together with local and neighborhood covariates $(\mathbf{X}_s, \mathbf{X}_{\mathcal{N}_s})$, into a latent embedding Z_s of the unobserved spatial field $U(s)$. The decoder

$$p_\psi(A_s \mid \mathbf{X}_s, \mathbf{X}_{\mathcal{N}_s}, Z_s) = \sigma(f_\psi(\mathbf{X}_s, \mathbf{X}_{\mathcal{N}_s}, Z_s)) \tag{7}$$

predicts A_s given covariates and the latent. To encode smoothness, we impose a Gaussian–Markov random-field prior $p_\theta(Z) = \mathcal{N}(\mathbf{0}, \tau^{-1}(L + \epsilon I)^{-1})$ with grid Laplacian L, or equivalently a deterministic penalty $\lambda Z^\top L Z$.

This CVAE is trained by minimizing

$$\mathcal{L}_A(\phi, \psi) = \sum_s \mathbb{E}_{q_\phi}\big[-\log p_\psi(A_s \mid \mathbf{X}_s, \mathbf{X}_{\mathcal{N}_s}, Z_s)\big] + \beta \sum_s D_{\mathrm{KL}}(q_\phi \| p_\psi), \tag{8}$$

with KL warm-up ($\beta \uparrow 1$). After convergence, we set $\hat{Z}_s = \mathbb{E}_{q_\phi}[Z_s]$ as the reconstructed confounder.

Stage ②: Potential outcome module. Given $\hat{Z}_s$, we estimate outcomes using a flexible function h:

$$\hat{Y}_s = h(A_s, A_{\mathcal{N}_s}, \mathbf{X}_s, \mathbf{X}_{\mathcal{N}_s}, \hat{Z}_s). \tag{9}$$

This module can be instantiated with any spatial model capable of handling interference and spatial confounding. For example, a U-Net architecture (Ronneberger et al., 2015) captures multi-scale spatial dependencies through an encoder–decoder with skip connections. Notably, Oprescu et al. (2025); Ali et al. (2024) use a U-Net to account for interference and spatial confounding in spatiotemporal settings. Other options include graph neural networks, patch-wise transformers, or classical spatial regression models, depending on the data modality.

Effect estimation proceeds by plug-in contrasts: the *direct effect* is

$$\hat{\tau}_{\mathrm{dir}} = \frac{1}{|\mathcal{S}|} \sum_{s \in \mathcal{S}} \Big[h(1, A_{\mathcal{N}_s}, \mathbf{X}_s, \mathbf{X}_{\mathcal{N}_s}, \hat{Z}_s) - h(0, A_{\mathcal{N}_s}, \mathbf{X}_s, \mathbf{X}_{\mathcal{N}_s}, \hat{Z}_s)\Big], \tag{10}$$

and analogously for spillover effects by varying $\mathbf{A}_{\mathcal{N}_s}$. Posterior draws of Z_s yield uncertainty bands.

Remark 1 (End-to-end variant). *One may train a single network by minimizing $\mathcal{L}_A + \gamma \mathcal{L}_Y$ while blocking gradients from $\mathcal{L}_Y$ into the CVAE. This preserves mediator avoidance while making the overall implementation and training more straightforward.*

Predictive checks. Following Rubin (1984), we assess whether the substitute confounder adequately explains the treatment assignment through posterior predictive checks. On a held-out validation set, we draw M replicated treatment vectors $\mathbf{a}^{(1)}, \ldots, \mathbf{a}^{(M)}$ from the decoder p_ψ and compare them against the observed assignment $\mathbf{a}$. Specifically, we compute the predictive p-value

$$p = \frac{1}{M} \sum_{m=1}^{M} \mathbf{1}\left\{ T(\mathbf{a}^{(m)}) < T(\mathbf{a}) \right\}, \tag{11}$$

where $T(\mathbf{a})$ is a discrepancy statistic measuring model fit. Following Wang and Blei (2019), we use

$$T(\mathbf{a}) = \mathbb{E}_{Z \sim q_\phi}[\log p_\psi(\mathbf{a} \mid \mathbf{X}, Z)], \tag{12}$$

the marginal log-likelihood of the observed assignment under the posterior distribution of Z. A value of p close to 0.5 indicates that the CVAE reproduces the treatment assignment distribution well, whereas extreme values signal model misspecification.

5 THEORETICAL PROPERTIES OF THE SPATIAL DECONFOUNDER

We now provide conditions under which the Spatial Deconfounder establishes causal identifiability of the direct and spillover effects in Equations (3) and (4). We begin with assumptions on consistency, positivity, and interference structure.

Assumption 1 (Spatial consistency). *The observed outcome equals the potential outcome under the assigned individual and neighborhood treatments. That is,*

$$Y_s = Y_s(a_s, \mathbf{a}_{\mathcal{N}_s}) \quad \text{if site } s \text{ receives treatment } a_s \text{ and its neighborhood } \mathcal{N}_s \text{ receives } \mathbf{a}_{\mathcal{N}_s}. \tag{13}$$

Assumption 2 (Spatial positivity). *For any site s, covariates $(\mathbf{X}_s, \mathbf{X}_{\mathcal{N}_s})$, and exposures $(a_s, \mathbf{a}_{\mathcal{N}_s})$, the probability of assignment is strictly positive: $0 < \Pr(a_s, \mathbf{a}_{\mathcal{N}_s} \mid \mathbf{X}_s, \mathbf{X}_{\mathcal{N}_s}) < 1$. Furthermore, we require* latent positivity *conditional on the Z, i.e., $0 < \Pr(a_s, \mathbf{a}_{\mathcal{N}_s} \mid \mathbf{X}_s, \mathbf{X}_{\mathcal{N}_s}, \mathbf{Z}_s) < 1$ if $\Pr(a_s, \mathbf{a}_{\mathcal{N}_s}, \mathbf{X}_s, \mathbf{X}_{\mathcal{N}_s}, \mathbf{Z}_s) > 0$.*

Assumption 3 (Localized interference).

Assumptions 1-3 are standard in the causal inference literature (e.g., Chen et al., 2024; Forastiere et al., 2021) and enable identification of the treatment effects. Classical approaches for treatment effect estimation in spatial settings additionally assume ignorability of the joint exposure given observed covariates. We relax this and allow for an unobserved latent field $U : \mathcal{S} \to \mathbb{R}^{d_U}$ spanning the grid. We only require that all confounders affecting purely local variation are observed in $(\mathbf{X}_s, \mathbf{X}_{\mathcal{N}_s})$. This assumption is weaker than full ignorability and is plausible in practice.

Assumption 4 (Latent field sufficiency). *There is no additional unobserved confounder $\tilde{U}$ that acts only on isolated regions. Formally, if*

$$(A_s, A_{\mathcal{N}_s}) \perp\!\!\!\perp Y_s(a, \mathbf{a}_{\mathcal{N}_s}) \mid \mathbf{X}_s, \mathbf{X}_{\mathcal{N}_s} \tag{14}$$

holds for some sites, then it holds uniformly across sites without conditioning on any extra $\tilde{U}$.

Assumption 4 is based on the standard assumption of single ignorability in the deconfounding literature (e.g., Bica et al., 2020) that requires that all confounders that only affect one single treatment are observed. This is necessary for reconstructing the unobserved confounder. In spatial causal inference, where units are interconnected, causal effects can be identified only if the confounding structure — observed and unobserved — is consistent across the entire lattice.

If the joint treatment distribution admits a factor model representation with the substitute confounder, then under Assumption 4 the joint assignment $(A_s, A_{\mathcal{N}_s})$ is ignorable given $(\mathbf{X}_s, \mathbf{X}_{\mathcal{N}_s}, Z_s)$. This follows from Proposition 5 in Wang and Blei (2019).

Finally, we assume the CVAE recovers a consistent proxy for the latent field.

Assumption 5 (Consistency of substitute confounder). *The encoder $q_\phi(z \mid a, \mathbf{a}_\mathcal{N}, \boldsymbol{x}, \boldsymbol{x}_\mathcal{N})$ converges to a degenerate distribution $\delta_{f_\phi(a, \mathbf{a}_\mathcal{N}, \boldsymbol{x}, \boldsymbol{x}_\mathcal{N})}$ for some deterministic function f_ϕ. Thus, Z_s is a deterministic function of the assigned causes and covariates.*

This assumption does not require the learned Z_s to equal the true unobserved confounder. It suffices that the CVAE learns a bijective transformation of the latent field (Wang and Blei, 2019).

Intuition. Under interference, each site's treatment is observed together with those of its neighbors. Because both A_s and $A_{\mathcal{N}_s}$ are influenced by the same smooth latent field $U(s)$, they provide multiple noisy "views" of that field. By fitting a factor model to the joint distribution of own and neighbor treatments, we reconstruct a substitute confounder Z_s that captures the underlying spatial structure. Conditioning on Z_s (together with observed covariates) restores ignorability, enabling unbiased estimation of direct and spillover effects.

Theorem 1 (Causal identifiability). *Suppose Assumptions 1–5 hold. Let Z be a piecewise constant function of the assigned causes and covariates $(a, \mathbf{a}_\mathcal{N}, \boldsymbol{x}, \boldsymbol{x}_\mathcal{N})$ and let the outcome be a separable function of the observed and unobserved variables*

$$\mathbb{E}_Y\big[Y_s(a, \mathbf{a}_\mathcal{N}) \mid \mathbf{X}_s = \boldsymbol{x}, \mathbf{X}_{\mathcal{N}_s} = \boldsymbol{x}_\mathcal{N}, Z_s = z\big] = f_1(a, \mathbf{a}_\mathcal{N}, \boldsymbol{x}, \boldsymbol{x}_\mathcal{N}) + f_2(z), \quad (15)$$

$$\mathbb{E}_Y\big[Y_s \mid A_s = a, \mathbf{A}_{\mathcal{N}_s} = \mathbf{a}_\mathcal{N}, \mathbf{X}_s = \boldsymbol{x}, \mathbf{X}_{\mathcal{N}_s} = \boldsymbol{x}_\mathcal{N}, Z_s = z\big] = f_3(a, \mathbf{a}_\mathcal{N}, \boldsymbol{x}, \boldsymbol{x}_\mathcal{N}) + f_4(z), \quad (16)$$

for continuously differentiable functions f_1, f_2, f_3, f_4. Consequently, the direct and spillover effects are identifiable as

$$\tau_{\text{dir}} = \mathbb{E}_{\mathbf{X}_s, \mathbf{X}_{\mathcal{N}_s}, Z}\Big[\mathbb{E}_Y\big[Y_s \mid A_s = 1, \mathbf{A}_{\mathcal{N}_s}, \mathbf{X}_s, \mathbf{X}_{\mathcal{N}_s}, Z_s\big] - \mathbb{E}_Y\big[Y_s \mid A_s = 0, \mathbf{A}_{\mathcal{N}_s}, \mathbf{X}_s, \mathbf{X}_{\mathcal{N}_s}, Z_s\big]\Big], \quad (17)$$

$$\tau_{\text{spill}} = \mathbb{E}_{\mathbf{X}_s, \mathbf{X}_{\mathcal{N}_s}, Z}\Big[\mathbb{E}_Y\big[Y_s \mid a, \mathbf{A}_{\mathcal{N}_s} = \mathbf{a}_{\mathcal{N}_s}^{(1)}, \mathbf{X}_s, \mathbf{X}_{\mathcal{N}_s}, Z_s\big] - \mathbb{E}_Y\big[Y_s \mid a, \mathbf{A}_{\mathcal{N}_s} = \mathbf{a}_{\mathcal{N}_s}^{(0)}, \mathbf{X}_s, \mathbf{X}_{\mathcal{N}_s}, Z_s\big]\Big].$$
$$(18)$$

Proof. The proof is provided in Section B. $\square$

6 EXPERIMENTS

We evaluate the Spatial Deconfounder on semi-synthetic datasets from the `SpaCE` benchmark (Tec et al., 2024), modified to incorporate both local interference and spatial confounding on real-world environmental data. To simulate unobserved confounding, we mask key covariates after data generation. We then compare different instantiations of our method against a range of spatial baselines under both local and spatial confounding scenarios. The section proceeds as follows: we describe the `SpaCE` environment and our data generation process, introduce the baselines and evaluation metrics, and finally interpret the results.

Additional details - including data generation, residual sampling, packages, hyperparameter tuning, and validation procedures - can be found in Section C. Replication code is available at `https://github.com/moprescu/Spatial-CI`.

Datasets and SpaCE Benchmark. We build on the `SpaCE` benchmark (Tec et al., 2024), which provides semi-synthetic spatial datasets for causal inference under unobserved confounding. In its original form, `SpaCE` simulates causal effects by masking important covariates in real-world environmental and health data, but it assumes independent treatments and does not account for interference between neighboring units. This makes it inadequate for evaluating methods, such as ours, that explicitly address both unobserved spatial confounding and localized spillovers.

To address this, we extend the `SpaCE` data generation process in two ways. First, we project the raw environmental data onto a uniform $0.25° \times 0.25°$ latitude–longitude grid, allowing convolutional architectures to exploit spatial locality while preserving large-scale patterns. Second, we incorporate *interference* into the potential outcome model by allowing outcomes to depend not only on local treatment A_s but also on neighbor treatments $A_{\mathcal{N}_s}$ within radius r_d. Specifically, we generate outcomes under two confounding regimes:

$$\text{(Local confounding)} \quad \hat{Y}_s = f(A_s, A_{\mathcal{N}_s}, X_s) + R_s, \quad (19)$$

$$\text{(Spatial confounding)} \quad \hat{Y}_s = f(A_s, A_{\mathcal{N}_s}, X_s, X_{\mathcal{N}_s}) + R_s, \quad (20)$$

Table 1: Performance under *local confounding*. Results averaged over 10 runs with 95% confidence intervals. r_d: neighborhood radius in data generation; R: neighborhood radius used by the deconfounder. Lower values indicate less bias.

ENVIRONMENT	CONFOUNDER	METHOD	DIR	SPILL
$PM_{2.5} \to m\ (r_d = 1)$	q_{SUMMER}	CVAE-SPATIAL+ (R=1)	**0.05 ± 0.02**	**0.31 ± 0.08**
		CVAE-SPATIAL+ (R=2)	0.13 ± 0.18	1.47 ± 1.91
		DAPSM	0.30 ± 0.03	N/A
		GCNN	0.41 ± 0.03	N/A
		S2SLS-LAG1	0.20 ± 0.00	N/A
		SPATIAL+	0.13 ± 0.04	N/A
		SPATIAL	0.10 ± 0.07	N/A
$PM_{2.5} \to m\ (r_d = 2)$	ρ_{POP}	CVAE-SPATIAL+ (R=1)	**0.03 ± 0.01**	0.23 ± 0.07
		CVAE-SPATIAL+ (R=2)	0.06 ± 0.03	**0.08 ± 0.04**
		DAPSM	0.16 ± 0.01	N/A
		GCNN	0.18 ± 0.03	N/A
		S2SLS-LAG1	0.07 ± 0.00	N/A
		SPATIAL+	0.10 ± 0.02	N/A
		SPATIAL	0.17 ± 0.03	N/A
$SO_4 \to PM_{2.5}\ (r_d = 1)$	NH_4	CVAE-SPATIAL+ (R=1)	0.08 ± 0.04	**0.71 ± 0.07**
		CVAE-SPATIAL+ (R=2)	**0.07 ± 0.04**	0.84 ± 0.08
		DAPSM	1.44 ± 0.00	N/A
		GCNN	0.52 ± 0.16	N/A
		S2SLS-LAG1	0.09 ± 0.00	N/A
		SPATIAL+	0.11 ± 0.03	N/A
		SPATIAL	0.08 ± 0.02	N/A
$SO_4 \to PM_{2.5}\ (r_d = 2)$	OC	CVAE-SPATIAL+ (R=1)	**0.09 ± 0.04**	**0.08 ± 0.03**
		CVAE-SPATIAL+ (R=2)	**0.09 ± 0.04**	0.52 ± 0.08
		DAPSM	1.24 ± 0.01	N/A
		GCNN	0.30 ± 0.10	N/A
		S2SLS-LAG1	0.21 ± 0.00	N/A
		SPATIAL+	0.13 ± 0.07	N/A
		SPATIAL	0.29 ± 0.01	N/A

where f is a predictive function learned from the observed data, X_s are observed covariates, and R_s are exogenous residuals. The local setting restricts confounding to site-level variables, while the spatial setting also allows neighborhood covariates to act as confounders.

Semi-synthetic data generation. To construct $\hat{Y}_s$, we proceed in four steps: (1) fit f using ensembles of machine learning models to predict observed outcomes Y_s, (2) compute residuals $\hat{R}_s = Y_s - f(\cdot)$ and estimate their spatial distribution P_R, (3) replace endogenous residuals with exogenous noise $R_s \sim P_R$, and (4) generate counterfactuals by varying local and neighbor treatments while holding confounders and residuals fixed. To simulate hidden confounding, we identify influential covariates by measuring the change in predictive performance when each is removed, then mask the most important ones at training and evaluation time.

Raw datasets. From the full SpaCE suite, we focus in the main text on two collections:

Air Pollution and Mortality: County-level data for the mainland US in 2010, including elderly mortality (CDC), fine particulate matter ($PM_{2.5}$) exposure (Di et al., 2019), behavioral risk factors (BRFSS) (Centers for Disease Control and Prevention, 2010), and Census demographics (U.S. Census Bureau, 2010). We study the effect of $PM_{2.5}$ exposure on mortality ($PM_{2.5} \to m$), with confounders such as *summer humidity* (q_{summer}) and *population density* (ρ_{pop}) masked.

$PM_{2.5}$ Components: High-resolution (1×1 km) gridded data on total $PM_{2.5}$ (Di et al., 2019) and its chemical composition (Amini et al., 2022), using annual averages for 2000. We focus on the effect of sulfate on overall $PM_{2.5}$ ($SO_4 \to PM_{2.5}$), with key latent drivers such as *ammonium* (NH_4) and *organic carbon* (OC) masked.

These two datasets provide complementary perspectives: the first captures socioeconomic and demographic confounding, while the second reflects atmospheric chemistry. Additional datasets and hidden-confounder variants are described in Appendix D.

Baselines and model variants. We benchmark against classical and modern spatial methods: S2SLS (Anselin, 1988) with outcome autoregression; spline-based SPATIAL and residualized SPATIAL+

Table 2: Performance under *spatial confounding*. Results averaged over 10 runs with 95% confidence intervals. r_d: neighborhood radius in data generation; R: neighborhood radius used by the deconfounder. Lower values indicate less bias.

ENVIRONMENT	CONFOUNDER	METHOD	DIR	SPILL
$PM_{2.5} \rightarrow m \ (r_d = 1)$	ρ_{POP}	CVAE-UNET (R=1)	0.04 ± 0.02	$\mathbf{0.10 \pm 0.03}$
		CVAE-UNET (R=2)	$\mathbf{0.03 \pm 0.01}$	0.12 ± 0.05
		DAPSM	0.20 ± 0.01	N/A
		GCNN	0.17 ± 0.06	N/A
		S2SLS-LAG1	0.05 ± 0.00	N/A
		SPATIAL+	0.27 ± 0.18	N/A
		SPATIAL	0.06 ± 0.06	N/A
		UNET	0.06 ± 0.01	0.17 ± 0.04
$SO_4 \rightarrow PM_{2.5} \ (r_d = 1)$	OC	CVAE-UNET (R=1)	$\mathbf{0.04 \pm 0.01}$	$\mathbf{0.05 \pm 0.01}$
		CVAE-UNET (R=2)	0.05 ± 0.02	0.05 ± 0.02
		DAPSM	1.57 ± 0.00	N/A
		GCNN	0.42 ± 0.15	N/A
		S2SLS-LAG1	0.13 ± 0.00	N/A
		SPATIAL+	0.06 ± 0.05	N/A
		SPATIAL	$\mathbf{0.04 \pm 0.01}$	N/A
		UNET	0.07 ± 0.02	0.05 ± 0.02

(Dupont et al., 2022); GCNN (Kipf, 2016) for non-linear neighbor aggregation; DAPSM (Papadogeorgou et al., 2019) for proximity-based matching; and UNET (Ronneberger et al., 2015), which can capture spillovers via neighbor treatments but does not adjust for hidden confounding.

For the *Spatial Deconfounder*, we instantiate the potential outcome module differently by setting the head to SPATIAL+ under local confounding (to ensure fairness) and to UNET under spatial confounding (to flexibly capture multi-scale structure). We also vary the neighborhood radius $r \in \{1, 2\}$ considered by the model and the latent confounder dimension in the CVAE ($d_Z \in \{1, 2, 4, 8, 16, 32\}$).

Evaluation metrics. We assess performance on the average direct effect (DIR) and spillover effect (SPILL). Following standard practice in causal inference (Hill, 2011; Shi et al., 2019; Cheng et al., 2022), we report standardized absolute bias, $\sigma_y^{-1} |\hat{\tau} - \tau|$, where τ is the true effect, $\hat{\tau}$ the estimate, and σ_y the outcome standard deviation. Standardization allows comparisons across datasets with different outcome scales.

Results. Tables 1 and 2 report performance under local and spatial confounding across different masked confounders (e.g., humidity, population density, ammonium, organic carbon). Across environments, the Spatial Deconfounder (CVAE) variants consistently achieve lower bias on direct effects than existing spatial baselines. Importantly, unlike most benchmarks, both CVAE and UNET can recover spillover effects, with CVAE generally providing more accurate estimates. Using UNET as the outcome head further strengthens spillover estimation, highlighting the benefit of spatial architectures when paired with deconfounding.

Additional experiments in Appendix D confirm these trends across broader settings. In a few cases where classical baselines perform comparably or slightly better, the scenarios involve very weak or extremely smooth confounding — conditions where stronger parametric assumptions may be advantageous. Overall, the results demonstrate that leveraging interference as a multi-cause signal yields substantial improvements in both direct and spillover effect estimation. These findings validate the core premise of the Spatial Deconfounder: interference can be exploited, rather than treated as a nuisance, to improve causal inference under unobserved confounding.

7 CONCLUSION

We introduce the **Spatial Deconfounder**, the first framework to jointly address interference and unobserved spatial confounding by treating neighborhood treatments as a multi-cause signal. A CVAE with a spatial prior reconstructs a substitute confounder, enabling estimation of direct and spillover effects with flexible outcome models. We prove identification under mild assumptions and demonstrate in semi-synthetic experiments derived from real environmental data that the method consistently reduces bias relative to existing spatial baselines.

Beyond methodological advances, our results highlight a conceptual shift: interference, often treated as a nuisance, can be exploited as a source of information about hidden structure. This perspective opens the door to more robust causal inference in complex spatial systems, with future extensions to spatiotemporal data, continuous treatments, and large-scale applications. Discussion of broader impacts and the use of LLMs in the preparation of this paper is provided in Section E.

8   ACKNOWLEDGMENTS

REFERENCES

S. Ali, O. Faruque, and J. Wang. Estimating direct and indirect causal effects of spatiotemporal interventions in presence of spatial interference. In *Joint European Conference on Machine Learning and Knowledge Discovery in Databases*, 2024.

H. Amini, M. Danesh-Yazdi, Q. Di, W. Requia, Y. Wei, Y. Abu-Awad, L. Shi, M. Franklin, C.-M. Kang, J. Wolfson, P. James, R. Habre, Q. Zhu, J. Apte, Z. Andersen, I. kloog, F. Dominici, P. Koutrakis, and J. Schwartz. Hyperlocal super-learned PM2.5 components across the contiguous us, 2022.

J. D. Angrist, G. W. Imbens, and D. B. Rubin. Identification of causal effects using instrumental variables. *Journal of the American Statistical Association*, 91(434):444–455, 1996.

L. Anselin. *Spatial Econometrics: Methods and Models*, volume 4. Springer Science & Business Media, 1988.

P. M. Aronow and C. Samii. Estimating average causal effects under general interference, with application to a social network experiment. *The Annals of Applied Statistics*, 11(4):1912—-1947, 2017.

I. Bica, A. Alaa, and M. Van Der Schaar. Time series deconfounder: Estimating treatment effects over time in the presence of hidden confounders. In *International conference on machine learning*, 2020.

Centers for Disease Control and Prevention. Behavioral risk factor surveillance system (BRFSS), 2010.

W. Chen, R. Cai, Z. Yang, J. Qiao, Y. Yan, Z. Li, and Z. Hao. Doubly robust causal effect estimation under networked interference via targeted learning. In *Proceedings of the 41st International Conference on Machine Learning*, 2024.

L. Cheng, R. Guo, R. Moraffah, P. Sheth, K. S. Candan, and H. Liu. Evaluation Methods and Measures for Causal Learning Algorithms . *IEEE Transactions on Artificial Intelligence*, 3(06): 924–943, 2022.

A. Curth, D. Svensson, J. Weatherall, and M. van der Schaar. Really doing great at estimating CATE? a critical look at ML benchmarking practices in treatment effect estimation. In *Advances Neural Information Processing Systems Datasets and Benchmarks Track (Round 2)*, 2021.

T. Deryugina, G. Heutel, N. H. Miller, D. Molitor, and J. Reif. The mortality and medical costs of air pollution: Evidence from changes in wind direction. *American Economic Review*, 109(12): 4178–4219, 2019.

Q. Di, H. Amini, L. Shi, I. Kloog, R. Silvern, J. Kelly, M. B. Sabath, C. Choirat, P. Koutrakis, A. Lyapustin, Y. Wang, L. J. Mickley, and J. Schwartz. An ensemble-based model of pm2.5 concentration across the contiguous united states with high spatiotemporal resolution. *Environment International*, 130:104909, 2019.

J. Dorn, K. Guo, and N. Kallus. Doubly-valid/doubly-sharp sensitivity analysis for causal inference with unmeasured confounding. *Journal of the American Statistical Association*, 120(549):331–342, 2025.

A. Dosovitskiy, L. Beyer, A. Kolesnikov, D. Weissenborn, X. Zhai, T. Unterthiner, M. Dehghani, M. Minderer, G. Heigold, S. Gelly, et al. An image is worth 16x16 words: Transformers for image recognition at scale. *arXiv preprint arXiv:2010.11929*, 2020.

E. Dupont, S. N. Wood, and N. H. Augustin. Spatial+: A novel approach to spatial confounding. *Biometrics*, 78(4):1279–1290, 2022.

N. Erickson, J. Mueller, A. Shirkov, H. Zhang, P. Larroy, M. Li, and A. Smola. Autogluon-tabular: Robust and accurate automl for structured data. *arXiv preprint arXiv:2003.06505*, 2020.

L. Forastiere, E. M. Airoldi, and F. Mealli. Identification and estimation of treatment and interference effects in observational studies on networks. *Journal of the American Statistical Association*, 116(534):901–918, 2021.

D. Frauen, V. Melnychuk, and S. Feuerriegel. Sharp bounds for generalized causal sensitivity analysis. *Advances in Neural Information Processing Systems*, 2023.

W. Hamilton, Z. Ying, and J. Leskovec. Inductive representation learning on large graphs. *Advances in Neural Information Processing Systems*, 2017.

E. M. Hanks, E. M. Schliep, M. B. Hooten, and J. A. Hoeting. Restricted spatial regression in practice: geostatistical models, confounding, and robustness under model misspecification. *Environmetrics*, 26(4):243–254, 2015.

T. Hatt and S. Feuerriegel. Sequential deconfounding for causal inference with unobserved confounders. In *Conference on Causal Learning and Reasoning*, 2024.

K. He, X. Zhang, S. Ren, and J. Sun. Deep residual learning for image recognition. In *IEEE Conference on Computer Vision and Pattern Recognition (CVPR)*, 2016.

I. Higgins, L. Matthey, A. Pal, C. Burgess, X. Glorot, M. Botvinick, S. Mohamed, and A. Lerchner. Beta-vae: Learning basic visual concepts with a constrained variational framework. In *International Conference on Learning Representations*, 2017.

J. L. Hill. Bayesian nonparametric modeling for causal inference. *Journal of Computational and Graphical Statistics*, 20(1):217–240, 2011.

J. Ho, A. Jain, and P. Abbeel. Denoising diffusion probabilistic models. In *Advances in Neural Information Processing Systems*, 2020.

J. S. Hodges and B. J. Reich. Adding spatially-correlated errors can mess up the fixed effect you love. *The American Statistician*, 64(4):325–334, 2010.

M. G. Hudgens and M. E. Halloran. Toward causal inference with interference. *Journal of the American Statistical Association*, 103(482):832–842, 2008.

G. W. Imbens and D. B. Rubin. *Causal inference in statistics, social, and biomedical sciences*. Cambridge University Press, 2015.

D. Kingma, T. Salimans, B. Poole, and J. Ho. Variational diffusion models. In *Advances in Neural Information Processing Systems*, 2021.

D. P. Kingma and M. Welling. Auto-encoding variational bayes. *International Conference on Learning Representations*, 2013.

T. Kipf. Semi-supervised classification with graph convolutional networks. *arXiv preprint arXiv:1609.02907*, 2016.

A. Larsen, S. Yang, B. J. Reich, and A. G. Rappold. A spatial causal analysis of wildland fire-contributed pm2. 5 using numerical model output. *The annals of applied statistics*, 16(4):2714, 2022.

R. Liaw, E. Liang, R. Nishihara, P. Moritz, J. E. Gonzalez, and I. Stoica. Tune: A research platform for distributed model selection and training, 2018.

Z. Liu, Y. Lin, Y. Cao, H. Hu, Y. Wei, Z. Zhang, S. Lin, and B. Guo. Swin transformer: Hierarchical vision transformer using shifted windows. In *IEEE/CVF International Conference on Computer Vision*, 2021.

L. Maaløe, C. K. Sønderby, S. K. Sønderby, and O. Winther. Auxiliary deep generative models. In *International Conference on Machine Learning*, 2016.

O. Oktay, J. Schlemper, L. L. Folgoc, M. Lee, M. Heinrich, K. Misawa, K. Mori, S. McDonagh, N. Y. Hammerla, B. Kainz, et al. Attention u-net: Learning where to look for the pancreas. *arXiv preprint arXiv:1804.03999*, 2018.

M. Oprescu, J. Dorn, M. Ghoummaid, A. Jesson, N. Kallus, and U. Shalit. B-learner: Quasi-oracle bounds on heterogeneous causal effects under hidden confounding. In *International Conference on Machine Learning*, 2023.

M. Oprescu, D. K. Park, X. Luo, S. Yoo, and N. Kallus. Gst-unet: Spatiotemporal causal inference with time-varying confounders. *arXiv preprint arXiv:2502.05295*, 2025.

G. Papadogeorgou and S. Samanta. Spatial causal inference in the presence of unmeasured confounding and interference. *arXiv preprint arXiv:2303.08218*, 2023.

G. Papadogeorgou, C. Choirat, and C. M. Zigler. Adjusting for unmeasured spatial confounding with distance adjusted propensity score matching. *Biostatistics*, 20(2):256–272, 2019.

D. Rezende and S. Mohamed. Variational inference with normalizing flows. In *International Conference on Machine Learning*, 2015.

D. J. Rezende, S. Mohamed, and D. Wierstra. Stochastic backpropagation and approximate inference in deep generative models. In *International Conference on Machine Learning*, 2014.

D. R. Roberts, V. Bahn, S. Ciuti, M. S. Boyce, J. Elith, G. Guillera-Arroita, S. Hauenstein, J. J. Lahoz-Monfort, B. Schröder, W. Thuiller, D. I. Warton, B. A. Wintle, F. Hartig, and C. F. Dormann. Cross-validation strategies for data with temporal, spatial, hierarchical, or phylogenetic structure. *Ecography*, 40(8):913–929, 2017.

O. Ronneberger, P. Fischer, and T. Brox. U-net: Convolutional networks for biomedical image segmentation. In *Medical Image Computing and Computer-Assisted Intervention – MICCAI 2015*, 2015.

D. B. Rubin. Bayesianly justifiable and relevant frequency calculations for the applied statistician. *The Annals of Statistics*, pages 1151–1172, 1984.

D. B. Rubin. Causal inference using potential outcomes: Design, modeling, decisions. *Journal of the American Statistical Association*, 100(469):322–331, 2005.

H. Rue and L. Held. *Gaussian Markov random fields: theory and applications*. Chapman and Hall/CRC, 2005.

C. Shi, D. M. Blei, and V. Veitch. Adapting neural networks for the estimation of treatment effects. In *Advances in Neural Information Processing Systems*, 2019.

X. Shi, Z. Chen, H. Wang, D.-Y. Yeung, W.-K. Wong, and W.-c. Woo. Convolutional lstm network: A machine learning approach for precipitation nowcasting. *Advances in Neural Information Processing Systems*, 2015.

M. E. Sobel. What do randomized studies of housing mobility demonstrate? causal inference in the face of interference. *Journal of the American Statistical Association*, 101(476):1398–1407, 2006.

K. Sohn, H. Lee, and X. Yan. Learning structured output representation using deep conditional generative models. *Advances in Neural Information Processing Systems*, 2015.

E. J. Tchetgen Tchetgen, I. R. Fulcher, and I. Shpitser. Auto-g-computation of causal effects on a network. *Journal of the American Statistical Association*, 116(534):833–844, 2021.

M. Tec, A. Trisovic, M. Audirac, S. Woodward, J. Hu, N. Khoshnevis, and F. Dominici. SpaCE: The spatial confounding environment. In *International Conference on Representation Learning*, 2024.

U.S. Census Bureau. 2010 census, 2010.

T. J. VanderWeele, E. J. T. Tchetgen, and M. E. Halloran. Interference and sensitivity analysis. *Statistical science: A Review Journal of the Institute of Mathematical Statistics*, 29(4):687, 2015.

P. Veličković, G. Cucurull, A. Casanova, A. Romero, P. Lio, and Y. Bengio. Graph attention networks. *arXiv preprint arXiv:1710.10903*, 2017.

Y. Wang and D. M. Blei. The blessings of multiple causes. *Journal of the American Statistical Association*, 114(528):1574–1596, 2019.

C. Zigler, V. Liu, F. Mealli, and L. Forastiere. Bipartite interference and air pollution transport: estimating health effects of power plant interventions. *Biostatistics*, 26(1):kxae051, 2025.

A EXTENDED LITERATURE REVIEW

The **Spatial Deconfounder** draws on three strands of prior work: (i) spatial causal inference under interference and spatially structured confounding, (ii) deconfounding methods for ATE estimation with unobserved confounders, and (iii) deep learning for spatial and latent structure modeling. We detail each in the sections that follow.

A.1 SPATIAL CAUSAL INFERENCE UNDER INTERFERENCE AND SPATIALLY STRUCTURED CONFOUNDING

Classical spatial causal inference. Most estimators of direct and spillover effects assume that bias can be removed by conditioning on *observed* covariates (together with a specified exposure mapping or interference structure). Design-based work—grounded in exposure mappings, partial-interference designs, and randomization inference—derives estimators or hypothesis tests under known neighborhood or network structure (e.g., Hudgens and Halloran, 2008; Sobel, 2006; Aronow and Samii, 2017; Forastiere et al., 2021; Tchetgen Tchetgen et al., 2021). Model-based strategies then adjust for that structure while still relying on measured covariates or correct functional form: spatial autoregressive and two-stage least-squares estimators for spatial-lag/lagged-error models (Anselin, 1988), and spline/GAM or restricted spatial regression approaches that treat residual spatial trend as a nuisance to improve precision and approximate balance (e.g., Hanks et al., 2015). Deep graph/convolutional architectures can pool information across nearby units to improve prediction or imputation, but by themselves do not furnish identification without additional causal assumptions (Kipf, 2016). Domain-specific simulators (e.g., wildfire spread or atmospheric transport) encode spatial dependence through process-based physics and are often used as inputs to causal analyses, yet they typically still condition on observed drivers or require design-identifying assumptions (e.g. Larsen et al., 2022; Zigler et al., 2025). All of the above *presume exchangeability given observed covariates (or a valid design)*; if important spatial determinants of treatment and outcome are unmeasured, residual confounding bias can remain.

Spatial confounding and bias-adjustment methods. A growing literature tackles *unmeasured* spatial confounding directly. One family augments outcome models with latent spatial random effects (e.g., BYM/ICAR or GMRF priors) to soak up smooth hidden structure; this can reduce bias when the confounder is well captured by the basis, but may leave bias or distort fixed effects under misspecification (Rue and Held, 2005; Hodges and Reich, 2010). Restricted spatial regression and related orthogonalization schemes constrain the latent field away from covariates to mitigate bias (Hanks et al., 2015). Building on this idea, Dupont et al. (2022) (SPATIAL+) explicitly orthogonalizes spatial structure in the covariates from the outcome trend to purge bias from unmeasured *spatial* confounding. Propensity-score strategies that incorporate spatial proximity—such as distance-adjusted propensity score matching—aim to proxy smooth unmeasured confounders via geography (Papadogeorgou et al., 2019). Instrumental-variable designs exploit exogenous spatial shocks (e.g., wind direction, policy boundaries, thermal inversions) to identify causal effects despite hidden confounding, but require strong relevance/exclusion conditions that are difficult to validate under interference (e.g., Angrist et al., 1996; Imbens and Rubin, 2015; Deryugina et al., 2019). Finally, Bayesian frameworks that jointly model interference and latent spatial fields (e.g., Papadogeorgou and Samanta, 2023) achieve identification under specified priors and structural assumptions. In short, existing approaches either (i) assume smoothly varying latent fields or valid instruments or (ii) rely on strong parametric priors. None exploit interference patterns themselves as a *signal* for nonparametrically recovering the hidden confounder, nor do they aim to explicitly reconstruct the unobserved confounding process—a gap our Spatial Deconfounder addresses.

A.2 DECONFOUNDING METHODS FOR ATE ESTIMATION WITH UNOBSERVED CONFOUNDERS

When confounders are unmeasured, point identification of causal effects generally fails. One approach is to derive bounds through sensitivity analysis (e.g., VanderWeele et al., 2015; Dorn et al., 2025; Oprescu et al., 2023; Frauen et al., 2023), trading identifiability for robustness. Another is the *deconfounder* framework, which fits a factor model to multiple causes in order to infer a substitute for the latent confounder, thereby restoring point identification (Wang and Blei, 2019; Bica et al.,

2020; Hatt and Feuerriegel, 2024). This stream is closest in spirit to our work: like us, it leverages multiplicity of treatments as a proxy for hidden structure. However, existing deconfounder methods require datasets with many simultaneous treatments (e.g., recommender systems, panel data) and assume no interference. Our approach resolves both limitations: interference itself naturally generates multiple-cause treatment vectors, enabling latent field recovery even with a single treatment type.

A.3   DEEP LEARNING FOR SPATIAL AND LATENT STRUCTURE MODELING

Deep learning for spatial modeling.   Modern deep architectures capture rich spatial structure but, on their own, remain predictive rather than identifying. U-Nets and encoder–decoder variants model multi-scale patterns on grids (Ronneberger et al., 2015; Oktay et al., 2018); graph neural networks extend to irregular domains (Kipf, 2016; Hamilton et al., 2017; Veličković et al., 2017); and patch-wise transformers model long-range dependencies on images and geospatial rasters (Dosovitskiy et al., 2020; Liu et al., 2021). Spatiotemporal extensions (e.g., ConvLSTM and graph/vision transformers) further capture dynamics (Shi et al., 2015). These tools provide flexible representations but require additional causal structure for identification.

Deep latent-variable models.   Finally, conditional variational autoencoders (CVAEs) and related deep generative models are widely used for representation learning with latent factors (Kingma and Welling, 2013; Sohn et al., 2015). Beyond CVAEs, the broader family of latent-variable models includes variational autoencoders with structured priors (Rezende et al., 2014; Maaløe et al., 2016), disentangled representation learning (Higgins et al., 2017), normalizing flows (Rezende and Mohamed, 2015), and diffusion-based generative models (Ho et al., 2020; Kingma et al., 2021), all of which offer flexible ways to recover hidden structure from high-dimensional data. While these methods are not causal in themselves, they provide natural tools for reconstructing latent processes from observed multi-cause data. In our framework, a CVAE combined with a spatial prior enables smooth, nonparametric recovery of a substitute confounder from local treatment vectors, which is then used for causal identification. Other architectures (e.g., diffusion models or flow-based methods) could, in principle, be substituted, but the key contribution lies in adapting deep latent-factor reconstruction to the spatial interference setting, where treatments on neighboring units jointly reveal the latent field.

A.4   OUR WORK

Our contribution lies at the intersection of spatial causal inference, methods for deconfounding under unobserved confounding, and modern deep latent-variable modeling. Existing approaches to spatial interference either assume that all relevant confounders are observed, or else mitigate bias through strong structural assumptions and priors—for example, by imposing smooth latent fields, leveraging restrictive IV conditions, or specifying parametric Bayesian models. In parallel, the "deconfounder" framework demonstrates that multiplicity of causes can be exploited to infer substitutes for unobserved confounders, thereby restoring point identification; however, these methods are designed for i.i.d. settings with many simultaneous treatments (e.g., recommender systems, panels), and do not naturally extend to spatial domains where interference and locality are intrinsic.

The *Spatial Deconfounder* closes this gap. We treat interference itself as the source of multi-cause information: treatment vectors on a unit and its neighbors contain precisely the dependence needed to reveal the hidden confounding field. By training a CVAE with a spatial prior, we nonparametrically reconstruct a smooth latent confounder from these local treatment vectors. This substitute confounder can then be used to adjust for bias, enabling identification and estimation of both direct and spillover effects. Crucially, our method achieves this without committing to a fully specified latent-field model or relying on IV-style exclusion restrictions, thereby combining the flexibility of nonparametric deconfounding with the structural realities of spatial interference.

B PROOFS

We first provide background by stating supporting definitions and lemmas. Then we prove our main theorem on the identifiability of the treatment effects.

B.1 SUPPORTING LEMMAS AND DEFINITIONS

Definition 1 (Ignorability). *The grid treatment $(a_s, \mathbf{a}_{\mathcal{N}_s})$ is* ignorable *given $Z_s, \mathbf{X}_s, \mathbf{X}_{\mathcal{N}_s}$, if for all $s = 1, \ldots, n$ and for all $(a, \mathbf{a}_{\mathcal{N}}) \in \mathcal{A}^{|\mathcal{S}|}$*

$$(A_s, \mathbf{A}_{\mathcal{N}_s}) \perp\!\!\!\perp Y_s(a, \mathbf{a}_{\mathcal{N}}) \mid Z_s, \mathbf{X}_s, \mathbf{X}_{\mathcal{N}_s}. \tag{21}$$

Definition 2 (Factor models). *A factor model of the assigned spatial treatments is a latent-variable model*

$$p_\phi(z_{1:|\mathcal{S}|}, \boldsymbol{x}_{1:|\mathcal{S}|}, \boldsymbol{x}_{\mathcal{N}_{1:|\mathcal{S}|}}, a_{1:|\mathcal{S}|}, \mathbf{a}_{\mathcal{N}_{1:|\mathcal{S}|}}) \tag{22}$$

$$= p(z_{1:|\mathcal{S}|}, \boldsymbol{x}_{1:|\mathcal{S}|}, \boldsymbol{x}_{\mathcal{N}_{1:|\mathcal{S}|}}) \prod_{s=1}^{|\mathcal{S}|} p_\phi(a_s \mid z_s, \boldsymbol{x}_s, \boldsymbol{x}_{\mathcal{N}_s}) \prod_{k \in \mathcal{N}_s} p_\phi(a_k \mid z_s, \boldsymbol{x}_s, \boldsymbol{x}_{\mathcal{N}_s}) \tag{23}$$

rendering the assigned treatments conditionally independent.

Lemma 1. *For the relation between the substitute confounder and factor models, it holds under weak regularity conditions*

1. *Assume the true distributions of the treatments $p(a_{1:|\mathcal{S}|}, \mathbf{a}_{\mathcal{N}_{1:|\mathcal{S}|}})$ can be represented by a factor model employing the substitute confounder Z, i.e., $p_\phi(z_{1:|\mathcal{S}|}, \boldsymbol{x}_{1:|\mathcal{S}|}, \boldsymbol{x}_{\mathcal{N}_{1:|\mathcal{S}|}}, a_{1:|\mathcal{S}|}, \mathbf{a}_{\mathcal{N}_{1:|\mathcal{S}|}})$. With the assumption of latent field sufficiency (see Assumption 4), the assigned treatments $(a, \mathbf{a}_{\mathcal{N}})$ are ignorable given Z_s, $\mathbf{X}_s$, and $\mathbf{X}_{\mathcal{N}_s}$, i.e.,*

$$(A_s, \mathbf{A}_{\mathcal{N}_s}) \perp\!\!\!\perp Y_s(a, \mathbf{a}_{\mathcal{N}}) \mid Z_s, \mathbf{X}_s, \mathbf{X}_{\mathcal{N}_s}. \tag{24}$$

2. *A factor model that represents the distribution of the assigned treatments always exists.*

Proof. The statement follows from Proposition 5 in Wang and Blei (2019). □

B.2 PROOF OF THE MAIN THEOREM

Theorem 1 (Causal identifiability). *Suppose Assumptions 1–5 hold. Let Z be a piecewise constant function of the assigned causes and covariates $(a, \mathbf{a}_{\mathcal{N}}, \boldsymbol{x}, \boldsymbol{x}_{\mathcal{N}})$ and let the outcome be a separable function of the observed and unobserved variables*

$$\mathbb{E}_Y\big[Y_s(a, \mathbf{a}_{\mathcal{N}}) \mid \mathbf{X}_s = \boldsymbol{x}, \mathbf{X}_{\mathcal{N}_s} = \boldsymbol{x}_{\mathcal{N}}, Z_s = z\big] = f_1(a, \mathbf{a}_{\mathcal{N}}, \boldsymbol{x}, \boldsymbol{x}_{\mathcal{N}}) + f_2(z), \tag{15}$$

$$\mathbb{E}_Y\big[Y_s \mid A_s = a, \mathbf{A}_{\mathcal{N}_s} = \mathbf{a}_{\mathcal{N}}, \mathbf{X}_s = \boldsymbol{x}, \mathbf{X}_{\mathcal{N}_s} = \boldsymbol{x}_{\mathcal{N}}, Z_s = z\big] = f_3(a, \mathbf{a}_{\mathcal{N}}, \boldsymbol{x}, \boldsymbol{x}_{\mathcal{N}}) + f_4(z), \tag{16}$$

for continuously differentiable functions f_1, f_2, f_3, f_4. Consequently, the direct and spillover effects are identifiable as

$$\tau_{\mathrm{dir}} = \mathbb{E}_{\mathbf{X}_s, \mathbf{X}_{\mathcal{N}_s}, Z}\Big[\mathbb{E}_Y\big[Y_s \mid A_s = 1, \mathbf{A}_{\mathcal{N}_s}, \mathbf{X}_s, \mathbf{X}_{\mathcal{N}_s}, Z_s\big] - \mathbb{E}_Y\big[Y_s \mid A_s = 0, \mathbf{A}_{\mathcal{N}_s}, \mathbf{X}_s, \mathbf{X}_{\mathcal{N}_s}, Z_s\big]\Big], \tag{17}$$

$$\tau_{\mathrm{spill}} = \mathbb{E}_{\mathbf{X}_s, \mathbf{X}_{\mathcal{N}_s}, Z}\Big[\mathbb{E}_Y\big[Y_s \mid a, \mathbf{A}_{\mathcal{N}_s} = \mathbf{a}_{\mathcal{N}_s}^{(1)}, \mathbf{X}_s, \mathbf{X}_{\mathcal{N}_s}, Z_s\big] - \mathbb{E}_Y\big[Y_s \mid a, \mathbf{A}_{\mathcal{N}_s} = \mathbf{a}_{\mathcal{N}_s}^{(0)}, \mathbf{X}_s, \mathbf{X}_{\mathcal{N}_s}, Z_s\big]\Big]. \tag{18}$$

Proof. First, observe that by the power-property and the separability of the outcome, we have

$$\mathbb{E}_Y[Y_s(a, \mathbf{a}_{\mathcal{N}})] = \mathbb{E}_{\mathbf{X}, \mathbf{X}_{\mathcal{N}}, Z}\big[\mathbb{E}_Y[Y_s(a, \mathbf{a}_{\mathcal{N}}) \mid \mathbf{X}_s, \mathbf{X}_{\mathcal{N}_s}, Z_s]\big] \tag{25}$$

$$= \mathbb{E}_{\mathbf{X}, \mathbf{X}_{\mathcal{N}}}[f_1(a, \mathbf{a}_{\mathcal{N}}, \mathbf{X}_s, \mathbf{X}_{\mathcal{N}_s})] + \mathbb{E}_Z[f_2(Z_s)]. \tag{26}$$

For the direct and indirect effects τ_{dir} and τ_{ind} follows

$$\tau_{dir} = \mathbb{E}_{\mathbf{X},\mathbf{x}_\mathcal{N}}[f_1(A_s = 1, \mathbf{a}_{\mathcal{N}_s}, \mathbf{X}_s, \mathbf{X}_{\mathcal{N}_s})] - \mathbb{E}_{\mathbf{X},\mathbf{x}_\mathcal{N}}[f_1(A_s = 0, \mathbf{a}_{\mathcal{N}_s}, \mathbf{X}_s, \mathbf{X}_{\mathcal{N}_s})] \tag{27}$$

$$= \int_{C(1,0)} \nabla_\nu \mathbb{E}_{\mathbf{X},\mathbf{x}_\mathcal{N}}[f_1(\nu, \mathbf{a}_\mathcal{N}, \mathbf{X}_s, \mathbf{X}_{\mathcal{N}_s})]d\nu, \quad \nu \in \mathbb{R} \tag{28}$$

and

$$\tau_{ind} = \mathbb{E}_{\mathbf{X},\mathbf{x}_\mathcal{N}}[f_1(a_s, \mathbf{A}_{\mathcal{N}_s} = \mathbf{a}_{\mathcal{N}_s}^{(1)}, \mathbf{X}_s, \mathbf{X}_{\mathcal{N}_s})] - \mathbb{E}_{\mathbf{X},\mathbf{x}_\mathcal{N}}[f_1(a_s, \mathbf{A}_{\mathcal{N}_s} = \mathbf{a}_{\mathcal{N}_s}^{(0)}, \mathbf{X}_s, \mathbf{X}_{\mathcal{N}_s})] \tag{29}$$

$$= \int_{C(a_{\mathcal{N}_s}^{(1)}, a_{\mathcal{N}_s}^{(0)})} \nabla_\kappa \mathbb{E}_{\mathbf{X},\mathbf{x}_\mathcal{N}}[f_1(a_s, \mathbf{A}_{\mathcal{N}_s} = \kappa, \mathbf{X}_s, \mathbf{X}_{\mathcal{N}_s})]d\kappa, \quad \kappa \in \mathbb{R}^{|\mathcal{S}|-1}. \tag{30}$$

We thus need to find an expression for the gradient to rewrite the integral in terms of observable quantities.

To do so, we first consider the conditional expected outcome. By Assumption 5 there exists a function g such that $Z = g(a, \mathbf{a}_\mathcal{N}, \mathbf{X}, \mathbf{X}_\mathcal{N})$. Therefore, it holds

$$\mathbb{E}_{\mathbf{X},\mathbf{x}_\mathcal{N},Z}\big[\mathbb{E}_Y[Y_s \mid A_s = a_s, \mathbf{A}_{\mathcal{N}_s} = \mathbf{a}_{\mathcal{N}_s}, \mathbf{X}_{\mathcal{N}_s}, Z_s]\big] \tag{31}$$

$$= \mathbb{E}_{\mathbf{X},\mathbf{x}_\mathcal{N}}\big[\mathbb{E}_Y[Y_s \mid A_s = a_s, \mathbf{A}_{\mathcal{N}_s} = \mathbf{a}_{\mathcal{N}_s}, \mathbf{X}_s, \mathbf{X}_{\mathcal{N}_s}, Z_s = g(a_s, \mathbf{a}_{\mathcal{N}_s}, \mathbf{X}_s, \mathbf{X}_{\mathcal{N}_s})]\big] \tag{32}$$

$$= \mathbb{E}_{\mathbf{X},\mathbf{x}_\mathcal{N}}\big[\mathbb{E}_Y[Y_s(a_s, \mathbf{a}_{\mathcal{N}_s}) \mid A_s = a_s, \mathbf{A}_{\mathcal{N}_s} = \mathbf{a}_{\mathcal{N}_s}, \mathbf{X}_s, \mathbf{X}_{\mathcal{N}_s}, Z_s = g(a_s, \mathbf{a}_{\mathcal{N}_s}, \mathbf{X}_s, \mathbf{X}_{\mathcal{N}_s})]\big], \tag{33}$$

where the latter equality follows from Assumption 1.

As $Y_s(a_s, \mathbf{a}_{\mathcal{N}_s}) \perp\!\!\!\perp A_s, \mathbf{A}_{\mathcal{N}_s} \mid \mathbf{X}_s, \mathbf{X}_{\mathcal{N}_s}, Z_s$ (by Lemma 1) and the outcomes are assumed to be separable, it follows

$$\mathbb{E}_{\mathbf{X},\mathbf{x}_\mathcal{N},Z}\big[\mathbb{E}_Y[Y_s \mid A_s = a_s, \mathbf{A}_{\mathcal{N}_s} = \mathbf{a}_{\mathcal{N}_s}, \mathbf{X}_s, \mathbf{X}_{\mathcal{N}_s}, Z_s]\big] \tag{34}$$

$$= \mathbb{E}_{\mathbf{X},\mathbf{x}_\mathcal{N}}\big[\mathbb{E}_Y[Y_s(a_s, \mathbf{a}_{\mathcal{N}_s}) \mid \mathbf{X}_s, \mathbf{X}_{\mathcal{N}_s}, Z_s = g(a_s, \mathbf{a}_{\mathcal{N}_s}, \mathbf{X}_s, \mathbf{X}_{\mathcal{N}_s})]\big] \tag{35}$$

$$= \mathbb{E}_{\mathbf{X},\mathbf{x}_\mathcal{N}}[f_1(a_s, \mathbf{a}_{\mathcal{N}_s}, \mathbf{X}_s, \mathbf{X}_{\mathcal{N}_s})] + \mathbb{E}_Z[f_2(g(a_s, \mathbf{a}_{\mathcal{N}_s}, \mathbf{X}_s, \mathbf{X}_{\mathcal{N}_s}))]. \tag{36}$$

Recall that by the definition of the conditional expected outcome, we have

$$\mathbb{E}_{\mathbf{X},\mathbf{x}_\mathcal{N},Z}\big[\mathbb{E}_Y[Y_s \mid A_s = a_s, \mathbf{A}_{\mathcal{N}_s} = \mathbf{a}_{\mathcal{N}_s}, \mathbf{X}_s, \mathbf{X}_{\mathcal{N}_s}, Z_s]\big] = \tag{37}$$

$$\mathbb{E}_{\mathbf{X},\mathbf{x}_\mathcal{N}}[f_3(a_s, \mathbf{a}_{\mathcal{N}_s}, \mathbf{X}_s, \mathbf{X}_{\mathcal{N}_s})] + \mathbb{E}_Z[f_4(g(a_s, \mathbf{a}_{\mathcal{N}_s}, \mathbf{X}_s, \mathbf{X}_{\mathcal{N}_s}))]. \tag{38}$$

Now, we are ready to consider the gradients in 29. Observe that for the gradients of the conditional outcome, it holds

$$\nabla_{a_s} \mathbb{E}_{\mathbf{X},\mathbf{x}_\mathcal{N},Z}\big[\mathbb{E}_Y[Y_s \mid a_s, \mathbf{A}_{\mathcal{N}_s} = \mathbf{a}_{\mathcal{N}_s}, \mathbf{X}_s, \mathbf{X}_{\mathcal{N}_s}, Z_s]\big] \tag{39}$$

$$= \nabla_{a_s} \mathbb{E}_{\mathbf{X},\mathbf{x}_\mathcal{N}}[f_1(a_s, \mathbf{a}_{\mathcal{N}_s}, \mathbf{X}_s, \mathbf{X}_{\mathcal{N}_s})] + \nabla_{a_s} \mathbb{E}_Z[f_2(g(a_s, \mathbf{a}_{\mathcal{N}_s}))] \tag{40}$$

$$= \nabla_{a_s} \mathbb{E}_{\mathbf{X},\mathbf{x}_\mathcal{N}}[f_3(a_s, \mathbf{a}_{\mathcal{N}_s}, \mathbf{X}_s, \mathbf{X}_{\mathcal{N}_s})] + \nabla_{a_s} \mathbb{E}_Z[f_4(g(a_s, \mathbf{a}_{\mathcal{N}_s}))] \tag{41}$$

with a similar expression for $\nabla_{\mathbf{a}_{\mathcal{N}_s}}$. Note that, up to a set of Lebesgue measure zero, the gradients of f_2 and f_4 disappear, i.e.,

$$\nabla_{a_s} \mathbb{E}_Z[f_2(g(a_s, \mathbf{a}_{\mathcal{N}_s}, \mathbf{X}_s, \mathbf{X}_{\mathcal{N}_s}))] = \nabla_{g(a_s, \mathbf{a}_{\mathcal{N}_s}, \mathbf{X}_s, \mathbf{X}_{\mathcal{N}_s})} f_2 \nabla_{a_s} g(a_s, \mathbf{a}_{\mathcal{N}_s}, \mathbf{X}_s, \mathbf{X}_{\mathcal{N}_s}) = 0 \tag{42}$$

and

$$\nabla_{a_s} \mathbb{E}_Z[f_4(g(a_s, \mathbf{a}_{\mathcal{N}_s}, \mathbf{X}_s, \mathbf{X}_{\mathcal{N}_s}))] = \nabla_{g(a_s, \mathbf{a}_{\mathcal{N}_s}, \mathbf{X}_s, \mathbf{X}_{\mathcal{N}_s})} f_4 \nabla_{a_s} g(a_s, \mathbf{a}_{\mathcal{N}_s}, \mathbf{X}_s, \mathbf{X}_{\mathcal{N}_s}) = 0 \tag{43}$$

as

$$\nabla_{a_s} g(a_s, \mathbf{a}_{\mathcal{N}_s}, \mathbf{X}_s, \mathbf{X}_{\mathcal{N}_s}) = 0.$$

Similarly,

$$\nabla_{\mathbf{a}_{\mathcal{N}_s}} \mathbb{E}_Z[f_2(g(a_s, \mathbf{a}_{\mathcal{N}_s}, \mathbf{X}_s, \mathbf{X}_{\mathcal{N}_s}))] = \nabla_{\mathbf{a}_{\mathcal{N}_s}} \mathbb{E}_Z[f_4(g(a_s, \mathbf{a}_{\mathcal{N}_s}, \mathbf{X}_s, \mathbf{X}_{\mathcal{N}_s}))] = 0.$$

Overall, we receive

$$\nabla_{a_s} \mathbb{E}_{\mathbf{X},\mathbf{x}_\mathcal{N}}[f_1(a_s, \mathbf{a}_{\mathcal{N}_s}, \mathbf{X}_s, \mathbf{X}_{\mathcal{N}_s})] = \nabla_{a_s} \mathbb{E}_{\mathbf{X},\mathbf{x}_\mathcal{N}}[f_3(a_s, \mathbf{a}_{\mathcal{N}_s}, \mathbf{X}_s, \mathbf{X}_{\mathcal{N}_s})] \tag{44}$$

and

$$\nabla_{\mathbf{a}_{\mathcal{N}_s}} \mathbb{E}_{\mathbf{X},\mathbf{x}_\mathcal{N}}[f_1(a_s, \mathbf{a}_{\mathcal{N}_s}, \mathbf{X}_s, \mathbf{X}_{\mathcal{N}_s})] = \nabla_{\mathbf{a}_{\mathcal{N}_s}} \mathbb{E}_{\mathbf{X},\mathbf{x}_\mathcal{N}}[f_3(a_s, \mathbf{a}_{\mathcal{N}_s}, \mathbf{X}_s, \mathbf{X}_{\mathcal{N}_s})]. \tag{45}$$

Finally, we can identify the direct treatment τ_{dir} effect as

$$\tau_{dir} = \int_{C(1,0)} \nabla_\nu \mathbb{E}_{\mathbf{X},\mathbf{X}_\mathcal{N}}[f_1(\nu, \mathbf{a}_\mathcal{N}, \mathbf{X}_s, \mathbf{X}_{\mathcal{N}_s})]d\nu, \quad \nu \in \mathbb{R} \tag{46}$$

$$= \int_{C(1,0)} \nabla_\nu \mathbb{E}_{\mathbf{X},\mathbf{X}_\mathcal{N}}[f_3(\nu, \mathbf{a}_\mathcal{N}, \mathbf{X}_s, \mathbf{X}_{\mathcal{N}_s})]d\nu, \quad \nu \in \mathbb{R} \tag{47}$$

$$= \mathbb{E}_{\mathbf{X},\mathbf{X}_\mathcal{N}}[f_3(A_s = 1, \mathbf{a}_\mathcal{N}, \mathbf{X}_s, \mathbf{X}_{\mathcal{N}_s})] - \mathbb{E}_{\mathbf{X},\mathbf{X}_\mathcal{N}}[f_3(A_s = 0, \mathbf{a}_\mathcal{N}, \mathbf{X}_s, \mathbf{X}_{\mathcal{N}_s})] \tag{48}$$

$$= \mathbb{E}_{\mathbf{X},\mathbf{X}_\mathcal{N}}[f_3(A_s = 1, \mathbf{a}_\mathcal{N}, \mathbf{X}_s, \mathbf{X}_{\mathcal{N}_s})] + \mathbb{E}_Z[f_4(Z_s)] \tag{49}$$

$$\quad - \mathbb{E}_{\mathbf{X},\mathbf{X}_\mathcal{N}}[f_3(A_s = 0, \mathbf{a}_\mathcal{N}, \mathbf{X}_s, \mathbf{X}_{\mathcal{N}_s})] - \mathbb{E}_Z[f_4(Z_s)] \tag{50}$$

$$= \mathbb{E}_{Z,\mathbf{X},\mathbf{X}_\mathcal{N}}\Big[\mathbb{E}_Y\big[Y_s \mid a_s=1, \mathbf{a}_{\mathcal{N}_s}, \mathbf{X}_s, \mathbf{X}_{\mathcal{N}_s}, Z_s\big] - \mathbb{E}_Y\big[Y_s \mid a_s=0, \mathbf{a}_{\mathcal{N}_s}, \mathbf{X}_s, \mathbf{X}_{\mathcal{N}_s}, Z_s\big]\Big] \tag{51}$$

and similarly the indirect treatment effect τ_{ind} as

$$\tau_{ind} = \int_{C(a_{\mathcal{N}_s}^{(1)}, a_{\mathcal{N}_s}^{(0)})} \nabla_\kappa \mathbb{E}_{\mathbf{X},\mathbf{X}_\mathcal{N}}[f_1(a_s, \mathbf{A}_{\mathcal{N}_s} = \kappa, \mathbf{X}_s, \mathbf{X}_{\mathcal{N}_s})]d\kappa \tag{52}$$

$$= \int_{C(a_{\mathcal{N}_s}^{(1)}, a_{\mathcal{N}_s}^{(0)})} \nabla_\kappa \mathbb{E}_{\mathbf{X},\mathbf{X}_\mathcal{N}}[f_3(a_s, \mathbf{A}_{\mathcal{N}_s} = \kappa, \mathbf{X}_s, \mathbf{X}_{\mathcal{N}_s})]d\kappa \tag{53}$$

$$= \mathbb{E}_{\mathbf{X},\mathbf{X}_\mathcal{N}}[f_3(a_s, \mathbf{a}_{\mathcal{N}_s}^{(1)}, \mathbf{X}_s, \mathbf{X}_{\mathcal{N}_s})] - \mathbb{E}_{\mathbf{X},\mathbf{X}_\mathcal{N}}[f_3(a_s, a_{\mathcal{N}_s}^{(0)}, \mathbf{X}_s, \mathbf{X}_{\mathcal{N}_s})] \tag{54}$$

$$= \mathbb{E}_{\mathbf{X},\mathbf{X}_\mathcal{N}}[f_3(a_s, \mathbf{a}_{\mathcal{N}_s}^{(1)}, \mathbf{X}_s, \mathbf{X}_{\mathcal{N}_s})] + \mathbb{E}_Z[f_4(Z_s)] \tag{55}$$

$$\quad - \mathbb{E}_{\mathbf{X},\mathbf{X}_\mathcal{N}}[f_3(a_s, \mathbf{a}_{\mathcal{N}_s}^{(0)}, \mathbf{X}_s, \mathbf{X}_{\mathcal{N}_s})] - \mathbb{E}_Z[f_4(Z_s)] \tag{56}$$

$$= \mathbb{E}_{Z,\mathbf{X},\mathbf{X}_\mathcal{N}}\Big[\mathbb{E}_Y\big[Y_s \mid a_s, \mathbf{a}_{\mathcal{N}_s}^{(1)}, \mathbf{X}_s, \mathbf{X}_{\mathcal{N}_s}, Z_s\big] - \mathbb{E}_Y\big[Y_s \mid a_s, \mathbf{a}_{\mathcal{N}_s}^{(0)}, \mathbf{X}_s, \mathbf{X}_{\mathcal{N}_s}, Z_s\big]\Big] \tag{57}$$

Overall, we proved that the substitute confounder generated by our spatial deconfounder renders the treatment effects identifiable. $\square$

C IMPLEMENTATION DETAILS

This section provides implementation details for our experimental setup. We cover four aspects:

1. **Semi-synthetic data generation:** construction of counterfactual outcomes under interference and spatial confounding using the `SpaCE` benchmark framework, with hidden confounders simulated by masking key covariates.
2. **Predictive model:** how the outcome model f is estimated with ensembles of machine-learning models, including convolutional networks for spatial structure.
3. **Software and hyperparameters:** the AutoML framework used for training and tuning, along with default settings.
4. **Benchmarks:** implementation details for baseline methods.

Semi-synthetic outcomes. Recall from Section 6 that we construct counterfactual outcomes via

$$\hat{Y}_s = f(A_s, \mathbf{A}_{\mathcal{N}_s}, \mathbf{X}_s) + R_s \quad \text{or} \quad \hat{Y}_s = f(A_s, \mathbf{A}_{\mathcal{N}_s}, \mathbf{X}_s, \mathbf{X}_{\mathcal{N}_s}) + R_s,$$

where f is a predictive model learned from real-world environmental data and R_s are exogenous, spatially correlated residuals with the same distribution as the endogenous residuals.

Predictive model with interference. We estimate f using ensembles of machine-learning models, with ensemble weights determined by predictive accuracy on held-out validation data. Following Tec et al. (2024) and the benchmarking guidelines of Curth et al. (2021), this avoids bias toward causal estimators tied to a single model class. To capture spatial structure, we include ResNet-18 (He et al., 2016) as one of the base learners. Training and hyperparameter tuning are automated with the `AutoGluon` Python package (Erickson et al., 2020), which performs model selection, hyperparameter search, and overfitting control with minimal human intervention. Default settings for `AutoGluon` are summarized in Table 3.

Table 3: Hyperparameters used in AutoML

Parameter	Value
package	AutoGluon v1.4.0
fit.presets	good_quality
fit.tuning_data	custom with algorithm 2
fit.use_bag_holdout	true
fit.time_limit	null
feature_importance.time_limit	900
hyperparameters	get_hyperparameter_config('multimodal')
hyperparameters.AG_AUTOMM.optim.max_epochs	10
hyperparameters.AG_AUTOMM.model.timm_image.checkpoint_name	resnet18

Spatially-aware train-validation split. We implement a *spatially-aware* train-validation data split (Roberts et al., 2017) that takes interference into account to avoid overfitting due to spatial correlations. We only consider nodes with complete neighborhoods for training and validation. This spatial splitting strategy identifies a limited number of validation nodes and applies breadth-first search to exclude their adjacent neighbors from the training dataset. For this study, we define each grid cell to have edges connecting it to its 8 surrounding cells. This algorithm is described in algorithm 2.

Synthetic Residual Generation. Following the approach established in Tec et al. (2024), we generate synthetic residuals using a Gaussian Markov Random Field (GMRF) from a spatial graph. Specifically, we sample the synthetic residuals according to: $\boldsymbol{R} \sim_{\text{iid}} \text{MultivariateNormal}(\mathbf{0}, \hat{\lambda}(\mathbb{D} - \hat{\rho}\mathbb{A}\mathbb{D})^{-1})$, where $\mathbb{A}$ represents the spatial graph's adjacency matrix, $\mathbb{D}$ denotes a diagonal matrix containing the degree (number of neighbors) for each spatial location, $\hat{\rho}$ parameterizes the spatial dependence between observations and their neighbors (estimated from the true residuals obtained from f), and $\hat{\lambda}$ is calibrated to preserve the exact variance of the observed residuals. We refer the reader to Tec et al. (2024) for additional details.

Benchmark Training and Hyperparameter Tuning. To ensure a fair comparison, we use the RAY TUNE (Liaw et al., 2018) framework for hyperparameter tuning. For all but DAPSM, the tuning metric is implemented as mean-squared error (MSE) from a validation set obtained with the spatially-aware splitting method in algorithm 2. We use this splitting algorithm for computing the tuning metric since random splitting would result in extreme overfitting (Roberts et al., 2017). For DAPSM we

---

Algorithm 2 Spatially-aware validation split selection with radius and complete neighborhoods

---

Input: Graph as map of neighbors $s \to \mathbb{N}_s$ where $\mathbb{N}_s \subset \mathbb{S}$ is the set of neighbors of s.
Params: Fraction α of seed validation points (default $\alpha = 0.02$); number of BFS levels L to include in the validation set (default $L = 1$); buffer size B indicating the number of BFS levels to leave outside training and validation (default $B = 1$); radius r_m of the model to consider when determining the split (default $r_m = 1$)
Output: Set of training nodes $\mathbb{T} \subset \mathbb{S}$ and validation nodes $\mathbb{V} \subset \mathbb{S}$.
 1: *# Helper function to check if node has complete r-hop neighborhood*
 2: **function** HASCOMPLETENEIGHBORHOOD(s, r):
 3:    expected_count $= (2r + 1)^2$ *# For square grid*
 4:    actual_neighbors $=$ GetNeighborsWithinRadius(s, r)
 5:    **return** |actual_neighbors| $=$ expected_count
 6: *# Filter to only nodes with complete neighborhoods*
 7: $\mathbb{S}_{valid} = \{s \in \mathbb{S} : $ HASCOMPLETENEIGHBORHOOD$(s, r_m)\}$
 8: *# Initialize validation set with seed nodes from valid nodes only*
 9: $\mathbb{V} =$ SampleWithoutReplacement$(\mathbb{S}_{valid}, \alpha)$
10: *# Expand validation set with neighbors*
11: **for** $\ell \in \{0, \ldots, L - 1\}$ **do**
12:    tmp $= \mathbb{V}$
13:    **for** $s \in$ tmp **do**
14:        $\mathbb{V} = \mathbb{V} \cup \mathbb{N}_s$
15:    **end for**
16: **end for**
17: *# Compute buffer*
18: $\mathbb{B} = \mathbb{V}$
19: **for** $b \in \{0, \ldots, B - 1 + r_m\}$ **do**
20:    tmp $= \mathbb{B}$
21:    **for** $s \in$ tmp **do**
22:        $\mathbb{B} = \mathbb{B} \cup \mathbb{N}_s$
23:    **end for**
24: **end for**
25: *# Exclude buffer for training set (from valid nodes only)*
26: $\mathbb{T} = \mathbb{S}_{valid} \setminus \mathbb{B}$
27: **return** $\mathbb{T}, \mathbb{V}$

---

use the covariate balance criterion following Papadogeorgou et al. (2019). After selecting the best hyperparameters, the method is retrained on the full data. Table 4 summarizes our hyperparameter search space for different baseline models. For CVAE models with radius R evaluated on a dataset of radius r_d, training and validation are restricted to nodes with radius $r_m = \max(r_d, \text{R})$. Each CVAE model also specifies a latent confounder dimension $d_Z \in \{1, 2, 4, 8, 16, 32\}$. The licenses of the data sources used for training are summarized in the supplement of Tec et al. (2024), which allow sharing and reuse for non-commercial purposes.

Model	Iterations	Tuning Metric	Value
CVAE-SPATIAL+	100	weight_decay_cvae beta_max (β) lam_t lam_y	loguniform between 1e-4 and 1e-3 loguniform between 1e-5 and 10 loguniform between 1e-5 and 1.0 loguniform between 1e-5 and 1.0
CVAE-UNET	60	weight_decay_cvae beta_max (β) weight_decay_head unet_base_chan	loguniform between 1e-4 and 1e-3 loguniform between 1e-3 and 1 loguniform between 1e-4 and 1e-3 16 or 32
DAPSM	N/A	propensity_score_penalty_value propensity_score_penalty_type spatial_weight	choose from [0.001, 0.01, 0.1, 1.0] l1 or l2 uniform between 0.0 and 1.0
GCNN	N/A	hidden_dim hidden_layers weight_decay lr epochs dropout	16 or 32 1 or 2 loguniform between 1e-6 and 1e-1 1e-3 or 3e-4 1000 or 2500 loguniform between 1e-3 to 0.5
SPATIAL+	2,500	lam_t lam_y	loguniform between 1e-5 and 1.0 loguniform between 1e-5 and 1.0
SPATIAL	2,500	lam	loguniform between 1e-5 and 1.0
UNET	50	unet_base_chan	choose from [8, 16, 32]

Table 4: Hyperparameter configurations evaluated for each model using a validation set. `Iterations` denotes the number of Ray Tune trials performed per model.

D FURTHER EXPERIMENTAL RESULTS

Our full experimental results are available for local confounding and spatial confounding at Table 5 and Table 6, respectively. There is a general pattern that CVAE models tend to outperform benchmarks in estimating direct effects. In particular, CVAE are the only local confounding methods that can also estimate spillover effects. In spatial confounding datasets with $r_d = 1$, deconfounders tend to have better direct effect and spillover estimation than UNET.

Table 5: Performance under *local confounding*. Results averaged over 10 runs with 95% confidence intervals. r_d: neighborhood radius in data generation; R: neighborhood radius used by the deconfounder. Lower values indicate less bias.

Environment	Confounder	Method	DIR	SPILL
$PM_{2.5} \rightarrow m$ ($r_d = 1$)	ρ_{pop}	CVAE-SPATIAL+ (R=0)	0.08 ± 0.06	n/a
		CVAE-SPATIAL+ (R=1)	0.06 ± 0.02	**0.30 ± 0.08**
		CVAE-SPATIAL+ (R=2)	0.04 ± 0.02	1.43 ± 1.90
		DAPSM	0.25 ± 0.01	n/a
		GCNN	0.36 ± 0.03	n/a
		S2SLS-LAG1	**0.03 ± 0.00**	n/a
		SPATIAL+	0.13 ± 0.04	n/a
		SPATIAL	0.10 ± 0.07	n/a
	q_{summer}	CVAE-SPATIAL+ (R=0)	0.09 ± 0.05	n/a
		CVAE-SPATIAL+ (R=1) (Z=2)	**0.05 ± 0.02**	**0.31 ± 0.08**
		CVAE-SPATIAL+ (R=2)	0.13 ± 0.18	1.47 ± 1.91
		DAPSM	0.30 ± 0.03	n/a
		GCNN	0.41 ± 0.03	n/a
		S2SLS-LAG1	0.20 ± 0.00	n/a
		SPATIAL+	0.13 ± 0.04	n/a
		SPATIAL	0.10 ± 0.07	n/a
$PM_{2.5} \rightarrow m$ ($r_d = 2$)	ρ_{pop}	CVAE-SPATIAL+ (R=0)	0.06 ± 0.02	n/a
		CVAE-SPATIAL+ (R=1)	**0.03 ± 0.01**	0.23 ± 0.07
		CVAE-SPATIAL+ (R=2)	0.06 ± 0.03	**0.08 ± 0.04**
		DAPSM	0.16 ± 0.01	n/a
		GCNN	0.18 ± 0.03	n/a
		S2SLS-LAG1	0.07 ± 0.00	n/a
		SPATIAL+	0.10 ± 0.02	n/a
		SPATIAL	0.17 ± 0.03	n/a
	q_{summer}	CVAE-SPATIAL+ (R=0)	**0.05 ± 0.02**	n/a
		CVAE-SPATIAL+ (R=1)	0.06 ± 0.02	0.10 ± 0.04
		CVAE-SPATIAL+ (R=2)	0.06 ± 0.02	**0.07 ± 0.03**

Environment	Confounder	Method	DIR	SPILL
		DAPSM	0.20 ± 0.01	n/a
		GCNN	0.16 ± 0.05	n/a
		S2SLS-LAG1	0.09 ± 0.00	n/a
		SPATIAL+	0.11 ± 0.02	n/a
		SPATIAL	0.17 ± 0.03	n/a
$SO_4 \rightarrow PM_{2.5}$ ($r_d = 1$)	NH_4	CVAE-SPATIAL+ (R=0)	0.09 ± 0.03	n/a
		CVAE-SPATIAL+ (R=1)	0.08 ± 0.04	**0.71 ± 0.07**
		CVAE-SPATIAL+ (R=2)	**0.07 ± 0.04**	0.84 ± 0.08
		DAPSM	1.44 ± 0.00	n/a
		GCNN	0.52 ± 0.16	n/a
		S2SLS-LAG1	0.09 ± 0.00	n/a
		SPATIAL+	0.11 ± 0.03	n/a
		SPATIAL	0.08 ± 0.02	n/a
	OC	CVAE-SPATIAL+ (R=0)	0.05 ± 0.02	n/a
		CVAE-SPATIAL+ (R=1)	0.06 ± 0.03	**0.65 ± 0.04**
		CVAE-SPATIAL+ (R=2)	0.07 ± 0.03	0.81 ± 0.10
		DAPSM	1.45 ± 0.00	n/a
		GCNN	0.77 ± 0.22	n/a
		S2SLS-LAG1	**0.00 ± 0.00**	n/a
		SPATIAL+	0.11 ± 0.03	n/a
		SPATIAL	0.08 ± 0.02	n/a
$SO_4 \rightarrow PM_{2.5}$ ($r_d = 2$)	NH_4	CVAE-SPATIAL+ (R=0)	0.11 ± 0.03	n/a
		CVAE-SPATIAL+ (R=1)	0.09 ± 0.03	**0.12 ± 0.05**
		CVAE-SPATIAL+ (R=2)	**0.08 ± 0.03**	0.35 ± 0.07
		DAPSM	1.23 ± 0.00	n/a
		GCNN	0.26 ± 0.09	n/a
		S2SLS-LAG1	0.10 ± 0.00	n/a
		SPATIAL+	0.13 ± 0.07	n/a
		SPATIAL	0.29 ± 0.01	n/a
	OC	CVAE-SPATIAL+ (R=0)	**0.08 ± 0.04**	n/a
		CVAE-SPATIAL+ (R=1)	0.09 ± 0.04	**0.08 ± 0.03**
		CVAE-SPATIAL+ (R=2)	0.12 ± 0.05	0.48 ± 0.11
		DAPSM	1.24 ± 0.01	n/a
		GCNN	0.30 ± 0.10	n/a
		S2SLS-LAG1	0.21 ± 0.00	n/a
		SPATIAL+	0.13 ± 0.07	n/a
		SPATIAL	0.29 ± 0.01	n/a

Table 6: Performance under *spatial confounding*. Results averaged over 10 runs with 95% confidence intervals. r_d: neighborhood radius in data generation; R: neighborhood radius used by the deconfounder. Lower values indicate less bias.

Environment	Confounder	Method	DIR	SPILL
$PM_{2.5} \rightarrow m$ ($r_d = 1$)	ρ_{pop}	CVAE-UNET (R=0)	0.05 ± 0.03	n/a
		CVAE-UNET (R=1)	0.04 ± 0.02	**0.10 ± 0.03**
		CVAE-UNET (R=2)	**0.03 ± 0.01**	0.12 ± 0.05
		DAPSM	0.20 ± 0.01	n/a
		GCNN	0.17 ± 0.06	n/a
		S2SLS-LAG1	0.05 ± 0.00	n/a
		SPATIAL+	0.27 ± 0.18	n/a
		SPATIAL	0.06 ± 0.06	n/a
		UNET	0.06 ± 0.01	0.17 ± 0.04
	q_{summer}	CVAE-UNET (R=0) (Z=1)	0.04 ± 0.03	n/a
		CVAE-UNET (R=1) (Z=32)	0.04 ± 0.01	**0.08 ± 0.04**
		CVAE-UNET (R=2) (Z=4)	**0.03 ± 0.01**	0.11 ± 0.04
		DAPSM	0.28 ± 0.04	n/a
		GCNN	0.23 ± 0.03	n/a
		S2SLS-LAG1	0.16 ± 0.00	n/a
		SPATIAL+	0.27 ± 0.18	n/a
		SPATIAL	0.07 ± 0.06	n/a
		UNET	0.04 ± 0.01	0.10 ± 0.05
$PM_{2.5} \rightarrow m$ ($r_d = 2$)	ρ_{pop}	CVAE-UNET (R=0)	0.09 ± 0.03	n/a
		CVAE-UNET (R=1)	0.14 ± 0.01	0.09 ± 0.05
		CVAE-UNET (R=2)	0.15 ± 0.01	**0.09 ± 0.04**
		DAPSM	0.15 ± 0.02	n/a
		GCNN	0.15 ± 0.04	n/a
		S2SLS-LAG1	0.06 ± 0.00	n/a
		SPATIAL+	0.08 ± 0.04	n/a
		SPATIAL	**0.05 ± 0.02**	n/a
		UNET	0.15 ± 0.01	0.15 ± 0.03
	q_{summer}	CVAE-UNET (R=0)	0.07 ± 0.03	n/a
		CVAE-UNET (R=1)	0.14 ± 0.01	**0.07 ± 0.03**
		CVAE-UNET (R=2)	0.15 ± 0.01	0.08 ± 0.04
		DAPSM	0.21 ± 0.01	n/a

		Method		
		GCNN	0.23 ± 0.03	n/a
		S2SLS-LAG1	0.10 ± 0.00	n/a
		SPATIAL+	0.07 ± 0.03	n/a
		SPATIAL	**0.05 ± 0.02**	n/a
		UNET	0.15 ± 0.00	0.08 ± 0.04
$SO_4 \to PM_{2.5}$ ($r_d = 1$)	NH_4	CVAE-UNET (R=0)	0.18 ± 0.01	n/a
		CVAE-UNET (R=1)	**0.02 ± 0.01**	**0.17 ± 0.02**
		CVAE-UNET (R=2)	0.04 ± 0.01	0.28 ± 0.03
		DAPSM	1.56 ± 0.00	n/a
		GCNN	0.55 ± 0.09	n/a
		S2SLS-LAG1	0.22 ± 0.00	n/a
		SPATIAL+	0.06 ± 0.05	n/a
		SPATIAL	0.04 ± 0.01	n/a
		UNET	0.04 ± 0.01	0.19 ± 0.04
	OC	CVAE-UNET (R=0) (Z=1)	0.04 ± 0.02	n/a
		CVAE-UNET (R=1) (Z=8)	**0.04 ± 0.01**	**0.05 ± 0.01**
		CVAE-UNET (R=2) (Z=16)	0.05 ± 0.01	0.17 ± 0.03
		DAPSM	1.57 ± 0.00	n/a
		GCNN	0.42 ± 0.15	n/a
		S2SLS-LAG1	0.13 ± 0.00	n/a
		SPATIAL+	0.06 ± 0.05	n/a
		SPATIAL	**0.04 ± 0.01**	n/a
		UNET	0.07 ± 0.02	0.05 ± 0.02
$SO_4 \to PM_{2.5}$ ($r_d = 2$)	NH_4	CVAE-UNET (R=0)	**0.03 ± 0.01**	n/a
		CVAE-UNET (R=1)	0.13 ± 0.01	**0.03 ± 0.01**
		CVAE-UNET (R=2)	0.14 ± 0.01	0.05 ± 0.02
		DAPSM	1.47 ± 0.00	n/a
		GCNN	0.66 ± 0.21	n/a
		S2SLS-LAG1	0.16 ± 0.00	n/a
		SPATIAL+	0.06 ± 0.02	n/a
		SPATIAL	0.06 ± 0.05	n/a
		UNET	0.15 ± 0.01	0.11 ± 0.04
	OC	CVAE-UNET (R=0)	0.06 ± 0.02	n/a
		CVAE-UNET (R=1)	0.15 ± 0.01	0.06 ± 0.04
		CVAE-UNET (R=2)	0.15 ± 0.00	**0.05 ± 0.02**
		DAPSM	1.49 ± 0.01	n/a
		GCNN	0.67 ± 0.12	n/a
		S2SLS-LAG1	0.09 ± 0.00	n/a
		SPATIAL+	**0.05 ± 0.02**	n/a
		SPATIAL	0.06 ± 0.05	n/a
		UNET	0.15 ± 0.01	0.08 ± 0.04

E BROADER IMPACTS AND LLM DISCLOSURE

Limitations While the Spatial Deconfounder advances identification and estimation under interference and unobserved spatial confounding, several limitations remain. First, our theoretical guarantees rely on assumptions such as localized interference and smooth latent confounders; these are useful but idealized and may not hold in domains with global spillovers or irregular hidden processes. Second, the framework is designed for gridded spatial data and assumes a regular lattice; extending to irregular spatial structures (e.g., graphs or administrative units) is an important direction for future work. Finally, although the CVAE prior aids in recovering latent structure, it may not fully capture unobserved confounders in extremely sparse or noisy data, and computational demands grow with grid size.

Broader impacts This work contributes to machine learning and causal inference by introducing a framework for more reliable effect estimation in spatial domains. Applications include environmental health, climate science, and social sciences, where accurate causal estimates can inform policy decisions. At the same time, we caution against uncritical use in high-stakes settings: violations of assumptions or biases in observational data may yield misleading conclusions. We encourage responsible deployment—especially in contexts affecting vulnerable populations—and recommend pairing our method with domain expertise, sensitivity analyses, and uncertainty quantification.

LLM usage disclosure. We used ChatGPT-5 and Claude Sonnet 4 to assist with editing, restructuring, and polishing the paper text. The authors carefully reviewed, revised, and validated all outputs to ensure alignment with the intended scientific content. All substantive contributions—conceptual framing, methodology, theoretical results, and experiments—are the work of the authors.